Journal of Theoretical and Applied Vibration and Acoustics 3(2) 165-198 (2017)

I S A V

Journal of Theoretical and Applied Vibration and Acoustics

journal homepage: http://tava.isav.ir

# Free vibration and wave propagation of thick plates using the generalized nonlocal strain gradient theory

**Seyed Mohammad Hossein Goushegir[a*], Shirko Faroughi[a]**

[a] *Faculty of Mechanical Engineering, Urmia University of Technology, Urmia, Iran*

ARTICLE INFO

*Article history:*
Received 3 August 2017

Received in revised form
9 December 2017

Accepted 23 December 2017

Available online 27 December 2017

*Keywords:*
Free vibration,

First-order shear deformation plate,

Wave propagation,

Higher-order nonlocal strain-gradient model,

Ritz method,

Wave.

ABSTRACT

In this paper, a size-dependent first-order shear deformation plate model is formulated in the framework of the higher-order generalized nonlocal strain-gradient (GNSG) theory. This model employs two nonlocal parameters and a strain-gradient coefficient to capture the both higher-order nonlocal stress-gradient and strain-gradient effects in nanostructures. The presence of these different scale parameters renders a unified model, which is able to predict both increase and reduction of stiffness in nanoplates. The governing equations are developed for free vibration of first-order shear deformation plates using Ritz method. The dispersion relations for the GNSG plate model is also derived. Several numerical examples are studied to show the efficiency, competence and accuracy of the proposed model. To ensure the applicability of the presented GNSG plate model, the results are compared with the experimental data available in the scientific literature. It is found that the effects of scale parameters on the wave frequencies are significant at high wavenumbers and ratio of any pair of these parameters is the main criterion for the correct study of size effects. The results show that the reduced nonlocal strain-gradient (RNSG) model and the GNSG model diverge in higher vibration modes.



## 1. Introduction

One of the challenges in nanotechnology is development and testing of nanostructures. Nano-scale materials such as graphene sheets are used in new sensors' design, gas detection and composite materials. This is due to their prominent mechanical, electronic and thermal properties

* Corresponding author:
*E-mail address*: smh.goushegir@mee.uut.ac.ir (S.M.H. Goushegir)

http://dx.doi.org/ 10.22064/tava. 2018.68796.1085

(Ruud e*t al*.[1]). Hence, studying graphene sheets is a key factor for researchers. Since the experiments at nano scales are difficult to conduct, the development of mathematical models and optimized solutions is an effective alternative. Generally three approaches have been used in the literature to analyze nanostructures, including: (a) atomistic modeling (Ball[2], Baughman *et al*.[3]), (b) hybrid atomistic–continuum mechanics (Bodily and Sun[4], Li and Chu [5]) and (c) continuum mechanics. Atomistic modeling and hybrid atomistic–continuum mechanics such as molecular dynamics (MD) (Liu and Wang[6]), molecular structural mechanics (MSM) (Shi and Zhao[7]) and density functional theory (Andres *et al*.[8]) are computationally expensive and can be applied only to a few atoms (or molecules), consequently continuum mechanics is widely used by researchers. The mechanical behavior of structures at nano scales is very different from their characteristics at large scales. Thus, instead of using classical continuum theory, which is not capable of predicting the effects of small scales in material, size-dependent continuum theories must be employed. The significant influence of the scale factors on the static and dynamic analysis of nanostructures is due to the fact that the lattice spacing between atoms is not negligible and the interatomic interactions in materials have a noticeable influence on the mechanical performance of nanostructures.

The nonlocal continuum field theory is originally developed by Eringen [9-11]. It is considered to be one the most popular non-classical theory in the research community. In this theory, the stress at a point ( $\boldsymbol{x}$ ) in a continuous domain is affected by both the strain tensor at that point and all other points of the body ( $\boldsymbol{x}'$ ). This nonlocal effect attenuates by a kernel function as the distance between the point ( $\boldsymbol{x}$ ) and the other points ( $\boldsymbol{x}'$ ) increases. Both experiment and molecular dynamics can determine a nonlocal parameter in this theory (Duan *et al*. [12], Wang *et al*.[13], Huang *et al*.[14], Liang and Han[15]). In fact, classical continuum theory can be transformed into differential-type nonlocal continuum theory by injecting a nonlocal parameter into the constitutive equations. For a special case of kernel function, the integral-type nonlocal elasticity (Pisano and Fuschi[16]) reduced to the Eringen's differential-type nonlocal elasticity Eringen [10]), which is extensively used in the literature due to its simplicity.

In the past researches, the differential-type nonlocal model has been widely used for bending, buckling and vibration analysis of nanoplates and nanobeams (Duan and Wang[17], Lu *et al*. [18], Aghababaei and Reddy [19], Thai [20]). Murmu and Pradhan[21] and Faroughi and Goushegir [22] have in vestigated the effect of small scales on the free in-plane vibration of homogeneous and heterogeneous nanoplates. Numerous applications of differential-type nonlocal continuum theory exist for investigating the dispersion of waves in carbon nano-tubes (CNTs) and graphene sheets (e.g., Wang *et al*.[23], Wang and Hu[24], Wang *et al*. [25]). According to these studies, the nonlocal size-dependent effect potentially has a fundamental role in studying the static and dynamic behavior of small-scale structures. The size-dependency of small-scale structures are not always accurately predictable by Eringen's nonlocal theory due to its limited capability of identifying size-dependent stiffness (Eltaher *et al*. [26], Lim *et al*. [27], Ma *et al*.[28]). For instance, the well-known paradoxical nonlocal cantilever beam problem has been studied by some researchers (Challamel & Wang[29], Challamel *et al*. [30], Wang *et al*.[31]) and an unreasonable stiffening effect was observed in their results for bending and free vibration of cantilever nanobeams. Likewise, the stiffness enhancement effects reported in experimental observations and the modified strain-gradient theory (Lam *et al*.[32]) are not well predictable by employing the Eringen's nonlocal elasticity model.

The equations of classical elasticity with additional higher-order strain-gradient terms are expanded by the gradient elasticity theories (Aifantis [33]). This is based on the hypothesis that the materials have to be considered as atoms with higher-order deformation mechanisms at micro- or nano scale and cannot be modeled as a set of points (Lim *et al*. [27]). In this theory, additional strain-gradient terms must be considered through the stress field. The gradient elasticity theory has been improved by Yang *et al*. [34]. The improved gradient elasticity theory states that the strain energy density should be defined as a function of both strain tensor and curvature tensor. These tensors conjugated with stress and couple stress tensors. Recently, the gradient elasticity theories has been extensively employed in the theoretical analysis of micro/nano- structures including bending, vibration and buckling of functionally graded beams (Reddy[35]), CNTs (Askes and Aifantis[36]), microtubules (Akgöz and Civalek [37]), rectangular nanoplates (Xu *et al*.[38]) and functionally graded microplates (Nguyen *et al*.[39]). The free vibration analysis of a functionally graded piezoelectric micro-scaled plate was implemented by Li and Pan [40] through the modified couple stress theory. In all of the above-mentioned references, a stiffness enhancement effect have been reported for these gradient elasticity models.

As discussed above, obviously two quite different size-dependent mechanical characteristics of materials at small scales are explained by the Eringen's differential-type nonlocal model and strain-gradient models. Recently Lim *et al*.[27] introduced a higher-order nonlocal strain-gradient theory that involves both of the scale parameters into a unified theory. Their goal was to determine the precise effects of the two scale parameters on the structural responses. Both the non-gradient nonlocal elastic stress field (Eringen's nonlocal model) and the nonlocal stress field of higher-order strain gradients are included in the stress tensor of the nonlocal strain-gradient theory. The nonlocal strain-gradient model contains two types of independent scale parameters including: material length scale parameter (strain-gradient parameter) and the nonlocal parameter. In recent years, many different scientific research have been done based on the higher-order strain-gradient theory introduced by Lim *et al*.[27] and their results were desirable. The nonlocal strain-gradient theory for beam-type structures provides an excellent matching with dispersion relations calculated by molecular dynamics simulations (e.g., Li and Hu[41], Li *et al*[42]. , Lim *et al*.[27]). Li and Hu[43] investigated the buckling of size-dependent nonlinear beams. Also a closed-form solution to the dispersion relations of wave propagation in fluid-conveying viscoelastic carbon nanotubes was developed by them (Li and Hu[41]). A higher-order nonlocal strain-gradient plate model for buckling of orthotropic nanoplates in a thermal environment has been developed by Farajpour *et al*. [44]. Li *et al*. [45] have analyzed the flexural wave propagation in small-scaled functionally graded beams. Li *et al*.[46] studied the free vibration of functionally graded nonlocal strain-gradient Timoshenko beams. Wave propagation in temperature- dependent inhomogeneous nanoplate was investigated by Ebrahimi *et al*. [47].

In this study, a size-dependent first-order shear deformation plate model is developed in the framework of generalized nonlocal strain-gradient (GNSG) theory. This theory is employed to investigate the free vibration and wave propagation of thick nanoplates. Two kinds of scale parameters, namely, the nonlocal parameters and the strain-gradient parameter are introduced to capture the size effects of materials in nanostructures. Then the GNSG model is used to illustrate both the increase and decrease of structural stiffness depending on the relative magnitudes for any pair of scale parameters. In the present analysis, the results obtained from the GNSG theory

are considered as the reference quantity in order to perform error analysis among the size-dependent continuum theories. Therefore, the classical continuum theory (CLT), pure nonlocal theory (PNL) and pure strain-gradient theory (PSG) are also investigated according to the GNSG theory and the relative errors are demonstrated efficiently for several types of boundary conditions, plate thicknesses and aspect ratios. The generalized eigenvalue problem for the free vibration of nanoplates is obtained by using a reliable and computationally efficient Ritz method based on boundary characteristic orthogonal polynomials (BCOPs). These polynomials have been generated through the Gram–Schmidt orthogonalization process. The advantage of these polynomials is that some of the entries of stiffness and mass matrices in the generalized eigenvalue problem become either zero or one due to the orthonormality of the assumed trial functions (Faroughi *et al.*[48]). The Ritz method has been extensively used in the vibration of nanoplates (e.g. Faroughi and Goushegir [22], Behera and Chakraverty [49], Behera and Chakraverty [50], Chakraverty and Behera [51]). A comprehensive analysis has been given on the dispersion relations of the wave propagation in GNSG plate model. Moreover, the effect of nonlocal parameters and the strain-gradient parameter on the dispersion relations of wave frequency, phase velocity and group velocity is demonstrated. Finally, the fronts of a single solitary flexural wave is illustrated for different types of size-dependent continuum theories as well as the GNSG theory.

## 2. Generalized higher-order nonlocal strain-gradient theory

According to the higher-order nonlocal strain-gradient theory developed by Lim *et al.* [27], the strain energy potential (*U)* is expressed as:

$$U = \frac{1}{2}\int_V \Bigg( C_{ijkl}\varepsilon_{ij}(\boldsymbol{x})\int_V \alpha_0\left(|\boldsymbol{x}'-\boldsymbol{x}|, e_0\xi\right)\varepsilon_{kl}(\boldsymbol{x}')dV(\boldsymbol{x}') + l^2 C_{ijkl}\varepsilon_{ij,m}(\boldsymbol{x})\int_V \alpha_1\left(|\boldsymbol{x}'-\boldsymbol{x}|, e_1\xi\right)\varepsilon_{kl,m}(\boldsymbol{x}')dV(\boldsymbol{x}')\Bigg)dV \tag{1}$$

where $C_{ijkl}$, $\varepsilon_{ij}$ and $\varepsilon_{ij,m}$ are the fourth-order elasticity tensor, strain tensor and first-order strain gradient, respectively. The strain-gradient parameter ($l$) is incorporated to characterize the significance of strain-gradient field and the nonlocal parameters $e_0\xi$ and $e_1\xi$ are introduced to describe the nonlocality of strain-gradient field, $\xi$ is an internal characteristic length, $e_0$ and $e_1$ are material constants that can be determined by curve fitting experimental data or by the results of molecular dynamics simulations. $|\boldsymbol{x}'-\boldsymbol{x}|$ represents the Euclidean distance between the points $\boldsymbol{x}$ and $\boldsymbol{x}'$. The functions $\alpha_0\left(|\boldsymbol{x}'-\boldsymbol{x}|, e_0\xi\right)$ and $\alpha_1\left(|\boldsymbol{x}'-\boldsymbol{x}|, e_1\xi\right)$ are the attenuation (kernel) functions defined to create nonlocal effects in the classical stress tensor. The kernel function is a positive scalar function with a distance decaying profile, which in the limit of $e_i\xi \to 0$, it reverts to the Dirac-delta function as shown in Eq. (2).

$$\lim_{e_i a\to 0}\alpha_i\left(|\boldsymbol{x}'-\boldsymbol{x}|, e_i\xi\right) = \delta\left(|\boldsymbol{x}'-\boldsymbol{x}|\right), \quad i = 0,1 \tag{2}$$

Using Eq. (1), the classical stress tensor $\boldsymbol{\sigma}$ and the higher-order stress tensor $\boldsymbol{\sigma}^{(1)}$ are obtained as:

$$\boldsymbol{\sigma} = C_{ijkl}\int_V \alpha_0\left(\left|\boldsymbol{x}'-\boldsymbol{x}\right|,e_0\xi\right)\varepsilon_{kl}\left(\boldsymbol{x}'\right)dV\left(\boldsymbol{x}'\right) \tag{3-a}$$

$$\boldsymbol{\sigma}^{(1)} = l^2 C_{ijkl}\int_V \alpha_1\left(\left|\boldsymbol{x}'-\boldsymbol{x}\right|,e_1\xi\right)\varepsilon_{kl,m}\left(\boldsymbol{x}'\right)dV\left(\boldsymbol{x}'\right) \tag{3-b}$$

The total stress tensor $\mathbf{t}$ of the nonlocal strain-gradient theory, is related to $\boldsymbol{\sigma}$ and $\boldsymbol{\sigma}^{(1)}$ via the following equation:

$$\mathbf{t} = \boldsymbol{\sigma} - \nabla\boldsymbol{\sigma}^{(1)} \tag{4}$$

where $\nabla$ is the Laplacian operator. We assume that the nonlocal kernel functions $\alpha_0\left(\left|\boldsymbol{x}'-\boldsymbol{x}\right|,e_0\xi\right)$ and $\alpha_1\left(\left|\boldsymbol{x}'-\boldsymbol{x}\right|,e_1\xi\right)$ satisfy the conditions presented by Eringen[10], which means that the linear nonlocal differential operator can be expressed as follows:

$$\boldsymbol{\mathcal{L}}_i = 1-\left(e_i\xi\right)^2\nabla^2 \tag{5}$$

Applying the operators of Eq. (5) on both sides of Eq. (4), the constitutive equations based on the generalized nonlocal strain-gradient can be derived as follows:

$$\begin{aligned}&\left[1-\left(e_1\xi\right)^2\nabla^2\right]\left[1-\left(e_0\xi\right)^2\nabla^2\right]\mathbf{t}_{ij}\\&\quad= C_{ijkl}\left[1-\left(e_1\xi\right)^2\nabla^2\right]\varepsilon_{kl} - C_{ijkl}l^2\left[1-\left(e_0\xi\right)^2\nabla^2\right]\nabla^2\varepsilon_{kl}\end{aligned} \tag{6}$$

where $\nabla^2 = \dfrac{\partial^2}{\partial x^2}+\dfrac{\partial^2}{\partial y^2}$ is the two-dimensional differential operator. The Eq. (6) contains three scale parameters. $e_0\xi$ denotes the lower-order nonlocal parameter, $e_1\xi$ is the higher-order nonlocal parameter and $l$ is the strain-gradient parameter. By setting $l=0$ and $e_1\xi = 0$ the GNSG theory can be reduced to the PNL theory (Eringen [9-11] as shown in Eq. (7).

$$\left[1-\left(e_0\xi\right)^2\nabla^2\right]\mathbf{t}_{ij} = C_{ijkl}\varepsilon_{kl} \tag{7}$$

Setting $e_0\xi = e_1\xi = 0$ in Eq. (6), the PSG model (Mindlin [52, 53] ) can be derived as:

$$\mathbf{t}_{ij} = C_{ijkl}\varepsilon_{kl} - C_{ijkl}l^2\nabla^2\varepsilon_{kl} \tag{8}$$

It is worth stressing that by keeping terms of order $\mathcal{O}\left(\nabla^2\right)$ and setting $e_0\xi = e_1\xi = e\xi$ the reduced nonlocal strain-gradient (RNSG) model can be achieved as:

$$\left[1-\left(e\xi\right)^2\nabla^2\right]\mathbf{t}_{ij} = C_{ijkl}\left(1-l^2\nabla^2\right)\varepsilon_{kl} \tag{9}$$

In fact, the RNSG theory integrates the both pure nonlocal (PNL) theory and pure strain-gradient (PSG) theory in a unified nonlocal strain-gradient model with two scale parameters (i.e., $e\xi$ and $l$ ).

## 3. Generalized nonlocal strain-gradient plate model

In the following section, a generalized nonlocal strain-gradient (GNSG) continuum model is developed for the vibration analysis of graphene sheets. We consider a rectangular nanoplate of length $a$, width $b$, and constant thickness of $h$ under plane stress condition. The plate occupies the domain $\Omega=\{0\le x\le a,\ 0\le y\le b,\ -h/2\le z\le h/2\}$ as shown in Fig. 1.

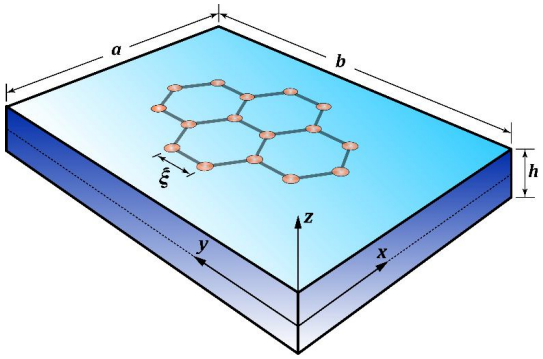


**Fig. 1** Geometry and dimensions of a thick nanoplate with an armchair lattice along x-axis

According to the first-order shear deformation (FSDT) plate theory, the displacement field of an arbitrary point $(x,y,z)$ within the domain $\Omega$ is expressed as (Wang *et. al*[54]):

$$\begin{aligned} u(x,y,z,t)&=u_0(x,y,t)+z\phi_x(x,y,t)\\ v(x,y,z,t)&=v_0(x,y,t)+z\phi_y(x,y,t)\\ w(x,y,z,t)&=w_0(x,y,t) \end{aligned} \tag{10}$$

where $u_0,v_0$ and $w_0$ denote the displacements in the middle surface of the nanoplate along $x$, $y$ and $z-$ directions, respectively; and $t$ represents the time in seconds. Also, $\phi_x$ and $\phi_y$ are the cross-sectional rotations of the mid-plane in $x$ and $y-$ directions. The strain-displacement relations are given by:

$$\{\epsilon\}=\{\epsilon^0\}+z\{\epsilon^1\} \tag{11}$$

The material property matrix for the orthotropic case is expressed as:

$$[\mathbb{D}]=\begin{bmatrix} Q_{11} & Q_{12} & 0 & 0 & 0\\ Q_{21} & Q_{22} & 0 & 0 & 0\\ 0 & 0 & Q_{66} & 0 & 0\\ 0 & 0 & 0 & Q_{44} & 0\\ 0 & 0 & 0 & 0 & Q_{55} \end{bmatrix} \tag{12}$$

$$Q_{11}=\frac{E_1}{1-\nu_{12}\nu_{21}}\ ,\ Q_{12}=Q_{21}=\frac{\nu_{12}E_2}{1-\nu_{12}\nu_{21}}\ ,\ Q_{22}=\frac{E_2}{1-\nu_{12}\nu_{21}}$$

$$\mathcal{Q}_{66} = G_{12} \quad , \quad \mathcal{Q}_{44} = G_{23}h \quad , \quad \mathcal{Q}_{55} = G_{13}h$$

The stress resultants in an orthotropic plate are related to the generalized displacements ($w_0, \phi_x, \phi_y$) by:

$$\begin{Bmatrix} \mathcal{M}_{xx} \\ \mathcal{M}_{yy} \\ \mathcal{M}_{xy} \\ \mathcal{S}_{yz} \\ \mathcal{S}_{xz} \end{Bmatrix} = \int_{-h/2}^{h/2} \begin{bmatrix} \mathcal{Q}_{11} & \mathcal{Q}_{12} & 0 & 0 & 0 \\ \mathcal{Q}_{12} & \mathcal{Q}_{22} & 0 & 0 & 0 \\ 0 & 0 & \mathcal{Q}_{66} & 0 & 0 \\ 0 & 0 & 0 & K_s\mathcal{Q}_{44} & 0 \\ 0 & 0 & 0 & 0 & K_s\mathcal{Q}_{55} \end{bmatrix} \begin{Bmatrix} z\dfrac{\partial \phi_x}{\partial x} \\ z\dfrac{\partial \phi_y}{\partial y} \\ z\left(\dfrac{\partial \phi_x}{\partial y} + \dfrac{\partial \phi_y}{\partial x}\right) \\ \dfrac{\partial w_0}{\partial y} + \phi_y \\ \dfrac{\partial w_0}{\partial x} + \phi_x \end{Bmatrix} dz \tag{13}$$

Using Eq. (6), the constitutive relations of an orthotropic plate based on the generalized nonlocal strain-gradient in Cartesian coordinates can be written in the following compact form:

$$\begin{gathered} \mathcal{L}_1\mathcal{L}_0 \mathrm{M}_{\alpha\beta} = \mathcal{L}_1 \mathcal{M}_{\alpha\beta} - \mathcal{L}_0 l^2 \nabla\cdot\nabla \mathcal{M}_{\alpha\beta} \\ \mathcal{L}_1\mathcal{L}_0 \mathrm{S}_{\alpha z} = \mathcal{L}_1 \mathcal{S}_{\alpha z} - \mathcal{L}_0 l^2 \nabla\cdot\nabla \mathcal{S}_{\alpha z} \\ \mathcal{L}_i = 1 - \left(e_i \xi\right)^2 \nabla^2 \\ i = 0,1 \text{ and } \alpha, \beta \equiv x, y \end{gathered} \tag{14}$$

The strain energy of the nanoplate is given by (Wang *et al*. [54]):

$$\mathbf{\Pi} = \frac{1}{2}\int_V \left[\mathbf{t}\right]\{\epsilon\}\, dV \tag{15}$$

The strain energy expression in terms of the plate nonlocal stress and strain fields (see, Eq. (11)) without any external forces is given by:

$$\mathbf{\Pi} = \frac{1}{2}\int_{\Omega}\left\{\int_{-h/2}^{h/2}\left[\mathrm{t}_{xx}\left(\epsilon_{xx}^0 + z\epsilon_{xx}^1\right) + \mathrm{t}_{yy}\left(\epsilon_{yy}^0 + z\epsilon_{yy}^1\right) + \mathrm{t}_{xy}\left(\gamma_{xy}^0 + z\gamma_{xy}^1\right) + \mathrm{t}_{xz}\gamma_{xz}^0 + \mathrm{t}_{yz}\gamma_{yz}^0\right]dz\right\}d\Omega \tag{16}$$

Integrating through the thickness of the plate model, we obtain:

$$\mathbf{\Pi} = \frac{1}{2}\int_{\Omega}\left[\mathrm{M}_{xx}\epsilon_{xx}^1 + \mathrm{M}_{yy}\epsilon_{yy}^1 + \mathrm{M}_{xy}\gamma_{xy}^1 + \mathrm{S}_{xz}\gamma_{xz}^0 + \mathrm{S}_{yz}\gamma_{yz}^0\right]d\Omega \tag{17}$$

where

$$\begin{Bmatrix} \mathrm{M}_{xx} \\ \mathrm{M}_{yy} \\ \mathrm{M}_{xy} \\ \mathrm{S}_{yz} \\ \mathrm{S}_{xz} \end{Bmatrix} = \Upsilon \begin{Bmatrix} \Xi_{11}\phi_{x,x} + \Xi_{12}\phi_{y,y} \\ \Xi_{12}\phi_{x,x} + \Xi_{22}\phi_{y,y} \\ \Xi_{66}\left(\phi_{x,y} + \phi_{y,x}\right) \\ \Xi_{44}\left(\phi_{y} + w_{0,y}\right) \\ \Xi_{55}\left(\phi_{x} + w_{0,x}\right) \end{Bmatrix}, \quad \Upsilon = \left[1 - \mu_1\nabla^2 - l^2\left(\nabla^2 - \mu_0\nabla^4\right)\right] \tag{18}$$

$$\Xi_{11} = \frac{1}{12}\mathcal{Q}_{11}h^3 \ , \ \Xi_{12} = \frac{1}{12}\mathcal{Q}_{12}h^3 \ , \ \Xi_{22} = \frac{1}{12}\mathcal{Q}_{22}h^3 \ ,$$

$$\Xi_{66} = \frac{1}{12}\mathcal{Q}_{66}h^3 \ , \ \Xi_{44} = K_s\mathcal{Q}_{44}h \ , \ \Xi_{55} = K_s\mathcal{Q}_{55}h$$

Here, $\mu_i = \left(e_i\xi\right)^2$ is a newly defined nonlocal parameter and $\Upsilon$ is a higher-order differential operator. Hence the strain energy of Eq. (17) for the present GNSG plate model can be obtained in the following form.

$$\begin{aligned} \boldsymbol{\Pi} = \frac{1}{2}\int_{\Omega}\Big\{\Big[ & \Upsilon\left(\Xi_{11}\phi_{x,x} + \Xi_{12}\phi_{y,y}\right)\phi_{x,x} + \Upsilon\left(\Xi_{12}\phi_{x,x} + \Xi_{22}\phi_{y,y}\right)\phi_{y,y} + \Xi_{66}\Upsilon\left(\phi_{x,y} + \phi_{y,x}\right)\left(\phi_{x,y} + \phi_{y,x}\right) \\ & + \Xi_{55}\Upsilon\left(\phi_{x} + w_{0,x}\right)\left(\phi_{x} + w_{0,x}\right) + \Xi_{44}\Upsilon\left(\phi_{y} + w_{0,y}\right)\left(\phi_{y} + w_{0,y}\right)\Big]\Big\}d\Omega \end{aligned} \tag{19}$$

To implement the Ritz procedure in the numerical example section, the bilinear symmetric form of the strain and functional is achieved by using the Green's first identity as below:

$$\begin{aligned} \boldsymbol{\Pi}_{\boldsymbol{b}} = \frac{1}{2}\int_{\Omega}\Big[ & \Xi_{11}\phi_{x,x}^2 + 2\Xi_{12}\phi_{x,x}\phi_{y,y} + \Xi_{22}\phi_{y,y}^2 + \Xi_{66}\left(\phi_{x,y} + \phi_{y,x}\right)^2 + \Xi_{55}\left(\phi_{x} + w_{0,x}\right)^2 + \Xi_{44}\left(\phi_{y} + w_{0,y}\right)^2 \\ & + \mu_1\Big(\Xi_{11}\nabla\phi_{x,x}\cdot\nabla\phi_{x,x} + 2\Xi_{12}\nabla\phi_{x,x}\cdot\nabla\phi_{y,y} + \Xi_{22}\nabla\phi_{y,y}\cdot\nabla\phi_{y,y} + \Xi_{66}\nabla\left(\phi_{x,y} + \phi_{y,x}\right)\cdot\nabla\left(\phi_{x,y} + \phi_{y,x}\right) \\ & + \Xi_{55}\nabla\left(\phi_{x} + w_{0,x}\right)\cdot\nabla\left(\phi_{x} + w_{0,x}\right) + \Xi_{44}\nabla\left(\phi_{y} + w_{0,y}\right)\cdot\nabla\left(\phi_{y} + w_{0,y}\right)\Big) \\ & + l^2\Big(\Xi_{11}\nabla\phi_{x,x}\cdot\nabla\phi_{x,x} + 2\Xi_{12}\nabla\phi_{x,x}\cdot\nabla\phi_{y,y} + \Xi_{22}\nabla\phi_{y,y}\cdot\nabla\phi_{y,y} + \Xi_{66}\nabla\left(\phi_{x,y} + \phi_{y,x}\right)\cdot\nabla\left(\phi_{x,y} + \phi_{y,x}\right) \\ & + \Xi_{55}\nabla\left(\phi_{x} + w_{0,x}\right)\cdot\nabla\left(\phi_{x} + w_{0,x}\right) + \Xi_{44}\nabla\left(\phi_{y} + w_{0,y}\right)\cdot\nabla\left(\phi_{y} + w_{0,y}\right) \\ & + \mu_0\Big(\Xi_{11}\nabla^2\phi_{x,x}\nabla^2\phi_{x,x} + 2\Xi_{12}\nabla^2\phi_{x,x}\nabla^2\phi_{y,y} + \Xi_{22}\nabla^2\phi_{y,y}\nabla^2\phi_{y,y} + \Xi_{66}\nabla^2\left(\phi_{x,y} + \phi_{y,x}\right)\nabla^2\left(\phi_{x,y} + \phi_{y,x}\right) \\ & + \Xi_{55}\nabla^2\left(\phi_{x} + w_{0,x}\right)\nabla^2\left(\phi_{x} + w_{0,x}\right) + \Xi_{44}\nabla^2\left(\phi_{y} + w_{0,y}\right)\nabla^2\left(\phi_{y} + w_{0,y}\right)\Big)\Big)\Big]d\Omega \end{aligned} \tag{20}$$

The Euler-Lagrange equations for the first-order shear deformation plate neglecting the in-plane displacements of the middle surface and external loads are given by (Wang *et al.*[54]):

$$
\begin{aligned}
&-\frac{1}{2}\oint_{\partial\Omega}\Big[\mu_1\left(\Xi_{11}\phi_{x,x}\nabla\phi_{x,x}+\Xi_{12}\left(\phi_{x,x}\nabla\phi_{y,y}+\phi_{y,y}\nabla\phi_{x,x}\right)+\Xi_{22}\phi_{y,y}\nabla\phi_{y,y}\right.\\
&+\Xi_{66}\left(\phi_{x,y}+\phi_{y,x}\right)\nabla\left(\phi_{x,y}+\phi_{y,x}\right)+\Xi_{55}\left(\phi_x+w_{0,x}\right)\nabla\left(\phi_x+w_{0,x}\right)+\Xi_{44}\left(\phi_y+w_{0,y}\right)\nabla\left(\phi_y+w_{0,y}\right)\Big)\\
&+l^2\left(\Xi_{11}\phi_{x,x}\nabla\phi_{x,x}+\Xi_{12}\left(\phi_{x,x}\nabla\phi_{y,y}+\phi_{y,y}\nabla\phi_{x,x}\right)+\Xi_{22}\phi_{y,y}\nabla\phi_{y,y}+\Xi_{66}\left(\phi_{x,y}+\phi_{y,x}\right)\nabla\left(\phi_{x,y}+\phi_{y,x}\right)\right.\\
&+\Xi_{55}\left(\phi_x+w_{0,x}\right)\nabla\left(\phi_x+w_{0,x}\right)+\Xi_{44}\left(\phi_y+w_{0,y}\right)\nabla\left(\phi_y+w_{0,y}\right)-\mu_0\Big(\Xi_{11}\left(\phi_{x,x}\nabla\left(\nabla^2\phi_{x,x}\right)-\nabla^2\phi_{x,x}\nabla\phi_{x,x}\right)\\
&+\Xi_{12}\left(\phi_{x,x}\nabla\left(\nabla^2\phi_{y,y}\right)-\nabla^2\phi_{y,y}\nabla\phi_{x,x}+\phi_{y,y}\nabla\left(\nabla^2\phi_{x,x}\right)-\nabla^2\phi_{x,x}\nabla\phi_{y,y}\right)+\Xi_{22}\left(\phi_{y,y}\nabla\left(\nabla^2\phi_{y,y}\right)-\nabla^2\phi_{y,y}\nabla\phi_{y,y}\right)\\
&+\Xi_{66}\left(\left(\phi_{x,y}+\phi_{y,x}\right)\nabla\left(\nabla^2\left(\phi_{x,y}+\phi_{y,x}\right)\right)-\nabla^2\left(\phi_{x,y}+\phi_{y,x}\right)\nabla\left(\phi_{x,y}+\phi_{y,x}\right)\right)\\
&+\Xi_{55}\left(\left(\phi_x+w_{0,x}\right)\nabla\left(\nabla^2\left(\phi_x+w_{0,x}\right)\right)-\nabla^2\left(\phi_x+w_{0,x}\right)\nabla\left(\phi_x+w_{0,x}\right)\right)\\
&\left.\left.\left.+\Xi_{44}\left(\left(\phi_y+w_{0,y}\right)\nabla\left(\nabla^2\left(\phi_y+w_{0,y}\right)\right)-\nabla^2\left(\phi_y+w_{0,y}\right)\nabla\left(\phi_y+w_{0,y}\right)\right)\right)\right)\Big]\cdot\hat{\mathbf{n}}\,d\Gamma
\end{aligned}
\tag{21}
$$

$$
\begin{aligned}
&\mathrm{M}_{xx,x}+\mathrm{M}_{xy,y}-\mathrm{S}_x=\mathrm{I}_2\phi_{x,tt}\\
&\mathrm{M}_{yy,y}+\mathrm{M}_{xy,x}-\mathrm{S}_y=\mathrm{I}_2\phi_{y,tt}\\
&\mathrm{S}_{x,x}+\mathrm{S}_{y,y}=\mathrm{I}_0 w_{0,tt}
\end{aligned}
\tag{22}
$$

Similarly, the bilinear symmetric form of the kinetic energy functional can be derived in the following form:

$$
\begin{aligned}
\mathbf{T}=&\frac{1}{2}\iint_{\Omega}\Big[\mathrm{I}_0 w_{0,t}^2+\mathrm{I}_2\left(\phi_{x,t}^2+\phi_{y,t}^2\right)\\
&-\left(\mu_0+\mu_1\right)\Big(\nabla^2\left(\mathrm{M}_{xx,x}+\mathrm{M}_{xy,y}-\mathrm{S}_x\right)\phi_x+\nabla^2\left(\mathrm{M}_{yy,y}+\mathrm{M}_{xy,x}-\mathrm{S}_y\right)\phi_y+\nabla^2\left(\mathrm{S}_{x,x}+\mathrm{S}_{y,y}\right)w_0\Big)\\
&+\mu_0\mu_1\Big(\nabla^4\left(\mathrm{M}_{xx,x}+\mathrm{M}_{xy,y}-\mathrm{S}_x\right)\phi_x+\nabla^4\left(\mathrm{M}_{yy,y}+\mathrm{M}_{xy,x}-\mathrm{S}_y\right)\phi_y+\nabla^4\left(\mathrm{S}_{x,x}+\mathrm{S}_{y,y}\right)w_0\Big)\Big]dxdy\\
&+\frac{1}{2}\int_{\partial\Omega}\Big[\left(\mu_0+\mu_1\right)\Big(\left(\nabla^2\mathrm{M}_{xx}\phi_x+\nabla^2\mathrm{M}_{xy}\phi_y+\nabla^2\mathrm{S}_x w_0\right)dy-\left(\nabla^2\mathrm{M}_{yy}\phi_y+\nabla^2\mathrm{M}_{xy}\phi_x+\nabla^2\mathrm{S}_y w_0\right)dx\Big)\\
&-\mu_0\mu_1\Big(\left(\nabla^4\mathrm{M}_{xx}\phi_x+\nabla^4\mathrm{M}_{xy}\phi_y+\nabla^4\mathrm{S}_x w_0\right)dy-\left(\nabla^4\mathrm{M}_{yy}\phi_y+\nabla^4\mathrm{M}_{xy}\phi_x+\nabla^4\mathrm{S}_y w_0\right)dx\Big)\Big]
\end{aligned}
\tag{23}
$$

In which $\omega$ is the angular frequency of the SHM.

Analytical solution of the present problem is very difficult. In this research, a numerical method that utilizes an efficient polynomial-based Ritz procedure is employed to determine the natural frequencies of the nanoplate.

$$\mathbf{T}_b = \frac{1}{2}\omega^2 \iint_{\Omega}\Big[ \mathrm{I}_2\left(\phi_x^2+\phi_y^2\right)+\mathrm{I}_0 w_0^2+\left(\mu_0+\mu_1\right)\Big(\mathrm{I}_2\left(\nabla\phi_x\cdot\nabla\phi_x+\nabla\phi_y\cdot\nabla\phi_y\right)+\mathrm{I}_0\nabla w_0\cdot\nabla w_0\Big)$$
$$+\mu_0\mu_1\left(\mathrm{I}_2\left(\nabla^2\phi_x\nabla^2\phi_x+\nabla^2\phi_y\nabla^2\phi_y\right)+\mathrm{I}_0\nabla^2 w_0\nabla^2 w_0\right)\Big]dxdy$$
$$+\frac{1}{2}\oint_{\partial\Omega}\Big[\left(\mu_0+\mu_1\right)\Big(\left(\nabla^2\mathrm{M}_{xx}\phi_x+\nabla^2\mathrm{M}_{xy}\phi_y+\nabla^2\mathrm{S}_x w_0\right)dy-\left(\nabla^2\mathrm{M}_{yy}\phi_y+\nabla^2\mathrm{M}_{xy}\phi_x+\nabla^2\mathrm{S}_y w_0\right)dx\Big)$$
$$-\mu_0\mu_1\Big(\left(\nabla^4\mathrm{M}_{xx}\phi_x+\nabla^4\mathrm{M}_{xy}\phi_y+\nabla^4\mathrm{S}_x w_0\right)dy-\left(\nabla^4\mathrm{M}_{yy}\phi_y+\nabla^4\mathrm{M}_{xy}\phi_x+\nabla^4\mathrm{S}_y w_0\right)dx\Big)\Big]$$
$$-\frac{1}{2}\oint_{\partial\Omega}\Big[\left(\mu_0+\mu_1\right)\Big(\mathrm{I}_2\left(\phi_x\nabla\phi_x+\phi_y\nabla\phi_y\right)+\mathrm{I}_0 w_0\nabla w_0\Big)$$
$$-\mu_0\mu_1\Big(\mathrm{I}_2\left(\phi_x\nabla\left(\nabla^2\phi_x\right)-\nabla^2\phi_x\nabla\phi_x+\phi_y\nabla\left(\nabla^2\phi_y\right)-\nabla^2\phi_y\nabla\phi_y\right)$$
$$+\mathrm{I}_0\left(w_0\nabla\left(\nabla^2 w_0\right)-\nabla^2 w_0\nabla w_0\right)\Big)\Big]\cdot\hat{\mathbf{n}}d\Gamma$$

**Table 1.** Gram-Schmidt orthonormalization procedure

| Step | Gram-Schmidt technique |
|---|---|
| **1** | $\mathcal{A}=\left(\frac{x}{a}\right)^{\Delta_1}\left(1-\frac{x}{a}\right)^{\Delta_3}$ <br> $\mathcal{B}=\left(\frac{y}{b}\right)^{\Delta_2}\left(1-\frac{y}{b}\right)^{\Delta_4}$ <br> $\mathcal{R}_i=\left\{1,x,y,x^2,xy,y^2,x^3,x^2y,xy^2,y^3,\ldots\right\}$ |
| **2** | $\mathcal{T}_i^{(\mathrm{z})}=\mathcal{AB}\mathcal{R}_i$ |
| **3** | $\Psi_1^{(\mathrm{z})}=\mathcal{T}_1^{(\mathrm{z})}$ <br> $\Psi_j^{(\mathrm{z})}=\mathcal{T}_i^{(\mathrm{z})}-\sum_{j=1}^{i-1}\mathrm{Y}_{ij}^{(\mathrm{z})}\Psi_j^{(\mathrm{z})}$ |
| **4** | $\mathrm{Y}_{ij}^{(\mathrm{z})}=\frac{\mathcal{T}_i^{(\mathrm{z})},\Psi_j^{(\mathrm{z})}}{\Psi_j^{(\mathrm{z})},\Psi_j^{(\mathrm{z})}}$ |
| **5** | $\left\langle\mathcal{T}_i^{(\mathrm{z})},\Psi_j^{(\mathrm{z})}\right\rangle=\int_0^b\int_0^a\mathcal{T}_i^{(\mathrm{z})}(x,y)\Psi_j^{(\mathrm{z})}(x,y)dxdy$ |
| **6** | $\tilde{\Psi}_i^{(\mathrm{z})}=\frac{\Psi_i^{(\mathrm{z})}}{\left\|\Psi_i^{(\mathrm{z})}\right\|}$ <br> $\left\|\Psi_i^{(\mathrm{z})}\right\|=\sqrt{\Psi_i^{(\mathrm{z})},\Psi_i^{(\mathrm{z})}}$ |

## 4. Solution procedure of the Ritz method

The Ritz trial functions for transverse deflection $W(x,y)$ and the cross-sectional rotations $\Phi_x(x,y)$ and $\Phi_y(x,y)$ are each expressed in terms of two-dimensional orthogonal polynomial functions sets as follows:

$$\begin{aligned} W(x,y) &= \sum_{i=1}^{N} \mathbb{W}_i \tilde{\Psi}_i^{(w)}(x,y) \\ \Phi_x(x,y) &= \sum_{i=1}^{N} \mathbb{X}_i \tilde{\Psi}_i^{(x)}(x,y) \\ \Phi_y(x,y) &= \sum_{i=1}^{N} \mathbb{Y}_i \tilde{\Psi}_i^{(y)}(x,y) \end{aligned} \tag{24}$$

In the Eq. (24), $\mathbb{W}_i$, $\mathbb{X}_i$ and $\mathbb{Y}_i$ are unknown coefficients, $N$ denotes the order of approximation in the discretization series. The functions $\tilde{\Psi}_i^{(w)}$, $\tilde{\Psi}_i^{(x)}$ and $\tilde{\Psi}_i^{(y)}$ are basis functions in the Ritz method obtained from the Gram-Schmidt ortho-normalization process through the steps shown in Table 1:

where $\mathsf{z} \equiv w,x,y$ and $\Delta_k$ ($k = 1,\ 2,\ 3$ and 4) represent the edge parameters controlling the boundary conditions of the rectangular GNSG plate model. Each of the edge parameters can be set to 0 and 1 for free ($F$), simply supported ($S$) and clamped ($C$) edge conditions as follow:

**Table 2.** Values of the edge parameter $\Delta_k$ for different types of boundary conditions

| $\Delta_k$ | **Transverse deflection** **Function:** $\tilde{\Psi}_i^{(w)}$ | **cross-sectional rotation** **functions:** $\tilde{\Psi}_i^{(x)}, \tilde{\Psi}_i^{(y)}$ |
|---|---|---|
| 0 | free ( $F$ ) | free ( $F$ ) or simply supported ( $S$ ) |
| 1 | simply supported ( $S$ ) or clamped ( $C$ ) | clamped ( $C$ ) |

Substituting Eq. (20) and Eq. (23) into the total energy functional ($\mathbf{\Pi}_b - \mathbf{T}_b$) and applying standard Ritz procedure to minimize the total energy with respect to the unknown coefficients yield:

$$\frac{\partial(\mathbf{\Pi}_b - \mathbf{T}_b)}{\partial \mathbb{W}_r}, \quad \frac{\partial(\mathbf{\Pi}_b - \mathbf{T}_b)}{\partial \mathbb{X}_r}, \quad \frac{\partial(\mathbf{\Pi}_b - \mathbf{T}_b)}{\partial \mathbb{Y}_r} \qquad r = 1,2,\ldots,\mathrm{N} \tag{25}$$

This leads to the eigenvalue equations in matrix form as shown in Eq. (26).

$$\left(\left[\mathbf{K}\right]-\omega^2\left[\mathbf{M}\right]\right)\begin{Bmatrix}\{\mathbf{W}\}\\ \{\mathbf{X}\}\\ \{\mathbf{Y}\}\end{Bmatrix}=0$$

$$\left[\mathbf{K}\right]=\begin{bmatrix}\left[\mathbf{k}_{ij}^{\mathrm{ww}}\right] & \left[\mathbf{k}_{ij}^{\mathrm{wx}}\right] & \left[\mathbf{k}_{ij}^{\mathrm{wy}}\right]\\ \left[\mathbf{k}_{ij}^{\mathrm{xw}}\right] & \left[\mathbf{k}_{ij}^{\mathrm{xx}}\right] & \left[\mathbf{k}_{ij}^{\mathrm{xy}}\right]\\ \left[\mathbf{k}_{ij}^{\mathrm{yw}}\right] & \left[\mathbf{k}_{ij}^{\mathrm{yx}}\right] & \left[\mathbf{k}_{ij}^{\mathrm{yy}}\right]\end{bmatrix},\quad \left[\mathbf{M}\right]=\begin{bmatrix}\left[\mathbf{m}_{ij}^{\mathrm{ww}}\right] & \left[\mathbf{O}\right] & \left[\mathbf{O}\right]\\ \left[\mathbf{O}\right] & \left[\mathbf{m}_{ij}^{\mathrm{xx}}\right] & \left[\mathbf{O}\right]\\ \left[\mathbf{O}\right] & \left[\mathbf{O}\right] & \left[\mathbf{m}_{ij}^{\mathrm{yy}}\right]\end{bmatrix} \tag{26}$$

where $\mathbf{K}$ and $\mathbf{M}$ are the $3\mathrm{N}\times 3\mathrm{N}$ symmetric positive-semidefinite stiffness and positive-definite mass matrices, respectively.

The entries of the symmetric nonlocal strain-gradient stiffness matrix ( $\mathbf{K}$ ) are given by:

$$\begin{aligned}\mathbf{k}_{ij}^{\mathrm{ww}} &= \int_0^b\int_0^a\Big[\Xi_{55}\tilde{\Psi}_{i,x}^{(w)}\tilde{\Psi}_{j,x}^{(w)}+\Xi_{44}\tilde{\Psi}_{i,y}^{(w)}\tilde{\Psi}_{j,y}^{(w)}+\mu_1\left(\Xi_{55}\nabla\tilde{\Psi}_{i,x}^{(w)}\cdot\nabla\tilde{\Psi}_{j,x}^{(w)}+\Xi_{44}\nabla\tilde{\Psi}_{i,y}^{(w)}\cdot\nabla\tilde{\Psi}_{j,y}^{(w)}\right)\\ &\quad+l^2\left(\Xi_{55}\nabla\tilde{\Psi}_{i,x}^{(w)}\cdot\nabla\tilde{\Psi}_{j,x}^{(w)}+\Xi_{44}\nabla\tilde{\Psi}_{i,y}^{(w)}\cdot\nabla\tilde{\Psi}_{j,y}^{(w)}+\mu_0\left(\Xi_{55}\nabla^2\tilde{\Psi}_{i,x}^{(w)}\nabla^2\tilde{\Psi}_{j,x}^{(w)}+\Xi_{44}\nabla^2\tilde{\Psi}_{i,y}^{(w)}\nabla^2\tilde{\Psi}_{j,y}^{(w)}\right)\right)\Big]dxdy\end{aligned}$$

$$\mathbf{k}_{ij}^{\mathrm{wx}} = \int_0^b\int_0^a\left[\Xi_{55}\tilde{\Psi}_{i,x}^{(w)}\tilde{\Psi}_{j}^{(x)}+\mu_1\left(\Xi_{55}\nabla\tilde{\Psi}_{i,x}^{(w)}\cdot\nabla\tilde{\Psi}_{j}^{(x)}\right)+l^2\left(\Xi_{55}\nabla\tilde{\Psi}_{i,x}^{(w)}\cdot\nabla\tilde{\Psi}_{j}^{(x)}+\mu_0\left(\Xi_{55}\nabla^2\tilde{\Psi}_{i,x}^{(w)}\nabla^2\tilde{\Psi}_{j}^{(x)}\right)\right)\right]dxdy$$

$$\mathbf{k}_{ij}^{\mathrm{wy}} = \int_0^b\int_0^a\left[\Xi_{44}\tilde{\Psi}_{i,y}^{(w)}\tilde{\Psi}_{j}^{(y)}+\mu_1\left(\Xi_{44}\nabla\tilde{\Psi}_{i,y}^{(w)}\cdot\nabla\tilde{\Psi}_{j}^{(y)}\right)+l^2\left(\Xi_{44}\nabla\tilde{\Psi}_{i,y}^{(w)}\cdot\nabla\tilde{\Psi}_{j}^{(y)}+\mu_0\left(\Xi_{44}\nabla^2\tilde{\Psi}_{i,y}^{(w)}\nabla^2\tilde{\Psi}_{j}^{(y)}\right)\right)\right]dxdy \tag{27}$$

$$\mathbf{k}_{ij}^{\mathrm{xw}} = \int_0^b\int_0^a\left[\Xi_{55}\tilde{\Psi}_{i}^{(x)}\tilde{\Psi}_{j,x}^{(w)}+\mu_1\left(\Xi_{55}\nabla\tilde{\Psi}_{i}^{(x)}\cdot\nabla\tilde{\Psi}_{j,x}^{(w)}\right)+l^2\left(\Xi_{55}\nabla\tilde{\Psi}_{i}^{(x)}\cdot\nabla\tilde{\Psi}_{j,x}^{(w)}+\mu_0\left(\Xi_{55}\nabla^2\tilde{\Psi}_{i}^{(x)}\nabla^2\tilde{\Psi}_{j,x}^{(w)}\right)\right)\right]dxdy$$

$$\begin{aligned}\mathbf{k}_{ij}^{\mathrm{xx}} &= \int_0^b\int_0^a\Big[\Xi_{11}\tilde{\Psi}_{i,x}^{(x)}\tilde{\Psi}_{j,x}^{(x)}+\Xi_{66}\tilde{\Psi}_{i,y}^{(x)}\tilde{\Psi}_{j,y}^{(x)}+\Xi_{55}\tilde{\Psi}_{i}^{(x)}\tilde{\Psi}_{j}^{(x)}\\ &\quad+\mu_1\left(\Xi_{11}\nabla\tilde{\Psi}_{i,x}^{(x)}\cdot\nabla\tilde{\Psi}_{j,x}^{(x)}+\Xi_{66}\nabla\tilde{\Psi}_{i,y}^{(x)}\cdot\nabla\tilde{\Psi}_{j,y}^{(x)}+\Xi_{55}\nabla\tilde{\Psi}_{i}^{(x)}\cdot\nabla\tilde{\Psi}_{j}^{(x)}\right)\\ &\quad+l^2\left(\Xi_{11}\nabla\tilde{\Psi}_{i,x}^{(x)}\cdot\nabla\tilde{\Psi}_{j,x}^{(x)}+\Xi_{66}\nabla\tilde{\Psi}_{i,y}^{(x)}\cdot\nabla\tilde{\Psi}_{j,y}^{(x)}+\Xi_{55}\nabla\tilde{\Psi}_{i}^{(x)}\cdot\nabla\tilde{\Psi}_{j}^{(x)}\right.\\ &\quad\left.+\mu_0\left(\Xi_{11}\nabla^2\tilde{\Psi}_{i,x}^{(x)}\nabla^2\tilde{\Psi}_{j,x}^{(x)}+\Xi_{66}\nabla^2\tilde{\Psi}_{i,y}^{(x)}\nabla^2\tilde{\Psi}_{j,y}^{(x)}+\Xi_{55}\nabla^2\tilde{\Psi}_{i}^{(x)}\nabla^2\tilde{\Psi}_{j}^{(x)}\right)\right)\Big]dxdy\end{aligned}$$

$$\begin{aligned}\mathbf{k}_{ij}^{\mathrm{xy}} &= \int_0^b\int_0^a\Big[\Xi_{12}\tilde{\Psi}_{i,x}^{(x)}\tilde{\Psi}_{j,y}^{(y)}+\Xi_{66}\tilde{\Psi}_{i,y}^{(x)}\tilde{\Psi}_{j,x}^{(y)}+\mu_1\left(\Xi_{12}\nabla\tilde{\Psi}_{i,x}^{(x)}\cdot\nabla\tilde{\Psi}_{j,y}^{(y)}+\Xi_{66}\nabla\tilde{\Psi}_{i,y}^{(x)}\cdot\nabla\tilde{\Psi}_{j,x}^{(y)}\right)\\ &\quad+l^2\left(\Xi_{12}\nabla\tilde{\Psi}_{i,x}^{(x)}\cdot\nabla\tilde{\Psi}_{j,y}^{(y)}+\Xi_{66}\nabla\tilde{\Psi}_{i,y}^{(x)}\cdot\nabla\tilde{\Psi}_{j,x}^{(y)}+\mu_0\left(\Xi_{12}\nabla^2\tilde{\Psi}_{i,x}^{(x)}\nabla^2\tilde{\Psi}_{j,y}^{(y)}+\Xi_{66}\nabla^2\tilde{\Psi}_{i,y}^{(x)}\nabla^2\tilde{\Psi}_{j,x}^{(y)}\right)\right)\Big]dxdy\end{aligned}$$

$$\mathbf{k}_{ij}^{\mathrm{yw}} = \int_0^b\int_0^a\left[\Xi_{44}\tilde{\Psi}_{i}^{(y)}\tilde{\Psi}_{j,y}^{(w)}+\mu_1\left(\Xi_{44}\nabla\tilde{\Psi}_{i}^{(y)}\cdot\nabla\tilde{\Psi}_{j,y}^{(w)}\right)+l^2\left(\Xi_{44}\nabla\tilde{\Psi}_{i}^{(y)}\cdot\nabla\tilde{\Psi}_{j,y}^{(w)}+\mu_0\left(\Xi_{44}\nabla^2\tilde{\Psi}_{i}^{(y)}\nabla^2\tilde{\Psi}_{j,y}^{(w)}\right)\right)\right]dxdy$$

$$\mathbf{k}_{ij}^{\mathrm{yx}}=\int_0^b\int_0^a\Big[\Xi_{12}\tilde{\Psi}_{i,y}^{(y)}\tilde{\Psi}_{j,x}^{(x)}+\Xi_{66}\tilde{\Psi}_{i,x}^{(y)}\tilde{\Psi}_{j,y}^{(x)}+\mu_1\left(\Xi_{12}\nabla\tilde{\Psi}_{i,y}^{(y)}\cdot\nabla\tilde{\Psi}_{j,x}^{(x)}+\Xi_{66}\nabla\tilde{\Psi}_{i,x}^{(y)}\cdot\nabla\tilde{\Psi}_{j,y}^{(x)}\right)$$
$$+l^2\left(\Xi_{12}\nabla\tilde{\Psi}_{i,y}^{(y)}\cdot\nabla\tilde{\Psi}_{j,x}^{(x)}+\Xi_{66}\nabla\tilde{\Psi}_{i,x}^{(y)}\cdot\nabla\tilde{\Psi}_{j,y}^{(x)}+\mu_0\left(\Xi_{12}\nabla^2\tilde{\Psi}_{i,y}^{(y)}\nabla^2\tilde{\Psi}_{j,x}^{(x)}+\Xi_{66}\nabla^2\tilde{\Psi}_{i,x}^{(y)}\nabla^2\tilde{\Psi}_{j,y}^{(x)}\right)\right)\Big]dxdy$$

$$\mathbf{k}_{ij}^{\mathrm{yy}}=\int_0^b\int_0^a\Big[\Xi_{22}\tilde{\Psi}_{i,y}^{(y)}\tilde{\Psi}_{j,y}^{(y)}+\Xi_{66}\tilde{\Psi}_{i,x}^{(y)}\tilde{\Psi}_{j,x}^{(y)}+\Xi_{44}\tilde{\Psi}_{i}^{(y)}\tilde{\Psi}_{j}^{(y)}$$
$$+\mu_1\left(\Xi_{22}\nabla\tilde{\Psi}_{i,y}^{(y)}\cdot\nabla\tilde{\Psi}_{j,y}^{(y)}+\Xi_{66}\nabla\tilde{\Psi}_{i,x}^{(y)}\cdot\nabla\tilde{\Psi}_{j,x}^{(y)}+\Xi_{44}\nabla\tilde{\Psi}_{i}^{(y)}\cdot\nabla\tilde{\Psi}_{j}^{(y)}\right)$$
$$+l^2\left(\Xi_{22}\nabla\tilde{\Psi}_{i,y}^{(y)}\cdot\nabla\tilde{\Psi}_{j,y}^{(y)}+\Xi_{66}\nabla\tilde{\Psi}_{i,x}^{(y)}\cdot\nabla\tilde{\Psi}_{j,x}^{(y)}+\Xi_{44}\nabla\tilde{\Psi}_{i}^{(y)}\cdot\nabla\tilde{\Psi}_{j}^{(y)}\right.$$
$$\left.+\mu_0\left(\Xi_{22}\nabla^2\tilde{\Psi}_{i,y}^{(y)}\nabla^2\tilde{\Psi}_{j,y}^{(y)}+\Xi_{66}\nabla^2\tilde{\Psi}_{i,x}^{(y)}\nabla^2\tilde{\Psi}_{j,x}^{(y)}+\Xi_{44}\nabla^2\tilde{\Psi}_{i}^{(y)}\nabla^2\tilde{\Psi}_{j}^{(y)}\right)\right)\Big]dxdy$$

And the entries of the symmetric higher-order nonlocal mass matrix ( $\mathbf{M}$ ) can be expressed in the form as follows:

$$\begin{aligned}
\mathbf{m}_{ij}^{\mathrm{ww}}&=\int_0^b\int_0^a \mathrm{I}_0\left(\tilde{\Psi}_i^{(w)}\tilde{\Psi}_j^{(w)}+\left(\mu_0+\mu_1\right)\nabla\tilde{\Psi}_i^{(w)}\cdot\nabla\tilde{\Psi}_j^{(w)}+\mu_0\mu_1\nabla^2\tilde{\Psi}_i^{(w)}\nabla^2\tilde{\Psi}_j^{(w)}\right)dxdy\\
\mathbf{m}_{ij}^{\mathrm{xx}}&=\int_0^b\int_0^a \mathrm{I}_2\left(\tilde{\Psi}_i^{(x)}\tilde{\Psi}_j^{(x)}+\left(\mu_0+\mu_1\right)\nabla\tilde{\Psi}_i^{(x)}\cdot\nabla\tilde{\Psi}_j^{(x)}+\mu_0\mu_1\nabla^2\tilde{\Psi}_i^{(x)}\nabla^2\tilde{\Psi}_j^{(x)}\right)dxdy\\
\mathbf{m}_{ij}^{\mathrm{yy}}&=\int_0^b\int_0^a \mathrm{I}_2\left(\tilde{\Psi}_i^{(y)}\tilde{\Psi}_j^{(y)}+\left(\mu_0+\mu_1\right)\nabla\tilde{\Psi}_i^{(y)}\cdot\nabla\tilde{\Psi}_j^{(y)}+\mu_0\mu_1\nabla^2\tilde{\Psi}_i^{(y)}\nabla^2\tilde{\Psi}_j^{(y)}\right)dxdy\\
&\left[\mathbf{O}\right]=\left[0\right]_{\mathrm{N}\times\mathrm{N}}
\end{aligned}\tag{28}$$

The unknown vectors $\{\mathbf{W}\}$, $\{\mathbf{X}\}$ and $\{\mathbf{Y}\}$ are given by:

$$\{\mathbf{W}\}=\{\mathbb{W}_1,\mathbb{W}_2,\ldots,\mathbb{W}_r\}^{\mathbf{T}},\{\mathbf{X}\}=\{\mathbb{X}_1,\mathbb{X}_2,\ldots,\mathbb{X}_r\}^{\mathbf{T}},\{\mathbf{Y}\}=\{\mathbb{Y}_1,\mathbb{Y}_2,\ldots,\mathbb{Y}_r\}^{\mathbf{T}}\quad r=1,2,\ldots,\mathrm{N}\tag{29}$$

where the superscript "T" denotes the transposition operator. By solving Eq. (26), the natural frequencies and related mode shapes of the proposed plate model can be obtained.

## 5. Dispersion relations of GNSG plate model

In order to obtain the dispersion relations of the GNSG plate model, the equations of motion based on the first-order shear deformation plate theory should be derived. By substituting Eq. (12) and Eq. (13) into Eq. (14) and then into the Eq. (22), the equations of motion for the first-order shear deformation plate based on the GNSG theory can be derived as follows:

$$\begin{aligned}
&\left[\mathcal{L}_1-\mathcal{L}_0l^2\nabla\cdot\nabla\right]\left(\Xi_{11}\phi_{x,xx}+\Xi_{12}\phi_{y,yx}+\Xi_{66}\left(\phi_{x,yy}+\phi_{y,xy}\right)-\Xi_{55}\left(\phi_x+w_{0,x}\right)\right)=\mathcal{L}_1\mathcal{L}_0\left(\mathrm{I}_2\phi_{x,tt}\right)\\
&\left[\mathcal{L}_1-\mathcal{L}_0l^2\nabla\cdot\nabla\right]\left(\Xi_{12}\phi_{x,xy}+\Xi_{22}\phi_{y,yy}+\Xi_{66}\left(\phi_{x,yx}+\phi_{y,xx}\right)-\Xi_{44}\left(\phi_y+w_{0,y}\right)\right)=\mathcal{L}_1\mathcal{L}_0\left(\mathrm{I}_2\phi_{y,tt}\right)
\end{aligned}\tag{30}$$

$$\left[\boldsymbol{\mathcal{L}}_1-\boldsymbol{\mathcal{L}}_0 l^2\nabla\cdot\nabla\right]\left(\Xi_{55}\left(\phi_{x,x}+w_{0,xx}\right)+\Xi_{44}\left(\phi_{y,y}+w_{0,yy}\right)\right)=\boldsymbol{\mathcal{L}}_1\boldsymbol{\mathcal{L}}_0\left(\mathrm{I}_0 w_{0,tt}\right)$$

where the coefficients $\Xi_{ij}$ are defined in earlier sections.

To study the wave propagation in nanoplates, the following harmonic functions are considered for the flexural waves and shear waves:

Flexural waves:

$$w_0\left(x,y,t\right)=\tilde{W}e^{i\left(-\omega t+k_x x+k_y y\right)} \tag{31}$$

Shear waves:

$$\phi_x\left(x,y,t\right)=\tilde{\Phi}_x e^{i\left(-\omega t+k_x x+k_y y\right)},\ \phi_y\left(x,y,t\right)=\tilde{\Phi}_y e^{i\left(-\omega t+k_x x+k_y y\right)}$$

Where, $\tilde{W}$, $\tilde{\Phi}_x$ and $\tilde{\Phi}_y$ represent the modal amplitudes of the flexural, and shear waves, $k_x$ and $k_y$ are the wave normal vector components of $\boldsymbol{k}=\left\langle k_x\ ,k_y\right\rangle$ along $x$ and $y-$ directions, respectively and $\omega$ is the wave frequency.

The substituting Eq. (31) into Eq. (30), yields the wave equation as follows:

$$\begin{bmatrix} A_{11} & A_{12} & A_{13} \\ -A_{12} & A_{22} & A_{23} \\ -A_{13} & A_{23} & A_{33} \end{bmatrix}\begin{Bmatrix} \tilde{W} \\ \tilde{\Phi}_x \\ \tilde{\Phi}_y \end{Bmatrix}=\begin{Bmatrix} 0 \\ 0 \\ 0 \end{Bmatrix} \tag{32}$$

Where, the entries of the $3\times3$ coefficient matrix ($\mathbf{A}$) are given as:

$$\begin{aligned}
A_{11}=&\left(\left(k_x^2+k_y^2+\mu_1\left(k_x^2+k_y^2\right)^2\right)\mu_0+1+\left(k_x^2+k_y^2\right)\mu_1\right)\mathrm{I}_0\omega^2\\
&+\Xi_{55}\left(\left(\left(-k_x^6-2k_x^4k_y^2-k_x^2k_y^4\right)\mu_0-k_x^4-k_x^2k_y^2\right)l^2-k_x^2+\left(-k_x^4-k_x^2k_y^2\right)\mu_1\right)\\
&+\Xi_{44}\left(\left(\left(-k_y^6-2k_x^2k_y^4-k_x^4k_y^2\right)\mu_0-k_y^4-k_x^2k_y^2\right)l^2-k_y^2+\left(-k_y^4-k_x^2k_y^2\right)\mu_1\right)\\
A_{12}=&\,i\Xi_{55}\left(\left(\left(k_x^5+2k_x^3k_y^2+k_xk_y^4\right)\mu_0+k_xk_y^2+k_x^3\right)l^2+k_x+\left(k_x^3+k_xk_y^2\right)\mu_1\right)\\
A_{13}=&\,i\Xi_{44}\left(\left(\left(k_y^5+2k_x^2k_y^3+k_yk_x^4\right)\mu_0+k_yk_x^2+k_y^3\right)l^2+k_y+\left(k_y^3+k_yk_x^2\right)\mu_1\right)\\
A_{22}=&\left(\left(k_x^2+k_y^2+\mu_1\left(k_x^2+k_y^2\right)^2\right)\mu_0+1+\left(k_x^2+k_y^2\right)\mu_1\right)\mathrm{I}_2\omega^2\\
&-\Xi_{11}\left(\left(\left(k_x^6+2k_x^4k_y^2+k_x^2k_y^4\right)\mu_0+k_x^4+k_x^2k_y^2\right)l^2+k_x^2+\left(k_x^4+k_x^2k_y^2\right)\mu_1\right)\\
&-\Xi_{55}\left(\left(\mu_0\left(k_x^2+k_y^2\right)^2+k_x^2+k_y^2\right)l^2+1+\mu_1\left(k_x^2+k_y^2\right)\right)\\
&-\Xi_{66}\left(\left(\left(k_y^6+2k_x^2k_y^4+k_x^4k_y^2\right)\mu_0+k_y^4+k_x^2k_y^2\right)l^2+k_y^2+\left(k_y^4+k_x^2k_y^2\right)\mu_1\right)
\end{aligned} \tag{33}$$

$$A_{23} = -\Xi_{12}\left(\left(\left(k_x k_y^5 + 2k_x^3 k_y^3 + k_x^5 k_y\right)\mu_0 + k_x^3 k_y + k_x k_y^3\right)l^2 + k_x k_y + \left(k_x^3 k_y + k_x k_y^3\right)\mu_1\right)$$
$$-\Xi_{66}\left(\left(\left(k_x k_y^5 + 2k_x^3 k_y^3 + k_x^5 k_y\right)\mu_0 + k_x^3 k_y + k_x k_y^3\right)l^2 + k_x k_y + \left(k_x^3 k_y + k_x k_y^3\right)\mu_1\right)$$

$$A_{33} = \left(\left(k_x^2 + k_y^2 + \mu_1\left(k_x^2 + k_y^2\right)^2\right)\mu_0 + 1 + \left(k_x^2 + k_y^2\right)\mu_1\right)\mathrm{I}_2\omega^2$$
$$-\Xi_{22}\left(\left(\left(k_y^6 + 2k_x^4 k_y^2 + k_x^2 k_y^4\right)\mu_0 + k_y^2 + \mu_1\left(k_y^4 + k_x^2 k_y^2\right)\right)l^2 + k_y^2 + \mu_1\left(k_y^4 + k_x^2 k_y^2\right)\right)$$
$$-\Xi_{44}\left(\left(k_x^2 + k_y^2 + \mu_0\left(k_x^2 + k_y^2\right)^2\right)l^2 + 1 + \mu_1\left(k_x^2 + k_y^2\right)\right)$$
$$-\Xi_{66}\left(\left(\left(k_x^6 + 2k_x^4 k_y^2 + k_x^2 k_y^4\right)\mu_0 + k_x^4 + k_x^2 k_y^2\right)l^2 + k_x^2 + \left(k_x^4 + k_x^2 k_y^2\right)\mu_1\right)$$

In continue, by equating the determinant of the matrix $\mathbf{A}$ of the Eq. (32) to zero the dispersion relations for different wave modes can be obtained.

The dispersion relation between wave frequency and other parameters can be shown in the form of real roots of a function explicitly as below:

$$\omega = \mathcal{H}\left(k_x, k_y, \mu_0, \mu_1, l\right) \tag{34}$$

Also, $\omega$ can be expressed as a function of wavenumber ($k$), which is more convenient and practical for analyses as below:

$$\omega = \mathcal{F}\left(k, \mu_0, \mu_1, l\right) \tag{35}$$

Where, $k = |\boldsymbol{k}| = \sqrt{k_x^2 + k_y^2}$ is the wavenumber, which is determined as $k = 2\pi/\lambda$ and $\lambda$ is the wavelength.

For plane waves, the phase velocity vector is defined as

$$\boldsymbol{c}_{\mathrm{P}} = \left(\omega / k^2\right)\boldsymbol{k} \tag{36}$$

Thus the magnitude of the phase velocity vector can be written as:

$$c_{\mathrm{P}} = \omega / k \tag{37-a}$$

The group velocity, which can be measured by tracking envelopes of a wave packet, is defined by:

$$c_{\mathrm{g}} = \mathrm{grad}_k \mathcal{F} = \partial\mathcal{F} / \partial k \tag{37-b}$$

## 6. Numerical results and discussion

### *6.1. Free vibration analysis*

#### *6.1.1. Validation*

To validate the proposed plate model, the natural frequencies of GNSG plates for two reduced cases are obtained using the present solution procedure and compared with those obtained by

Aghababaei and Reddy[19] and Shahriari *et al*. [55]. The free vibration of higher-order nonlocal strain-gradient plates considering first-order shear deformations has not been studied yet to the best of our knowledge. Hence, in order to verify the present higher-order nanostructured plate model, the left and right-hand side of Eq. (6) have been compared with the available results of the literature for pure nonlocal (PNL) and pure strain-gradient (PSG) cases, respectively. Aghababaei and Reddy [19] used the nonlocal linear elasticity theory of Eringen (see, pure nonlocal theory of Eq. (7)) to study the free vibration of nanoplates. Shahriari *et al*.[55] presented the free vibration analysis of carbon nanotube-reinforced composite (FG-CNTRC) nanoplates based on Mindlin's strain-gradient theory (see, pure strain-gradient theory of Eq. (8)).

**First case ( $\mu_1 = l = 0$ ):** The free vibration solution presented in Eq. (26) is numerically evaluated for an isotropic fully simply-supported nanoplate. Here, the presented formulation reduces to the pure nonlocal theory. In Table 3, the numerical results for classical and first-order shear deformation theory of plate are presented for the pure nonlocal case. The following parameters are used to obtain the numerical values (Aghababaei and Reddy [19]):

$$a = 10\,\text{nm}, E = 30\times10^6\ \text{Pa}, \nu = 0.3, \rho = 1 \tag{38}$$

where, $a$, $E$, $\nu$ and $\rho$ are plate length, Young's modules, Poisson's ratio and density of the plate, respectively. One may observe close agreement of the present results with those of Aghababaei and Reddy[19].

**Table 3.** Non-dimensional fundamental frequency $\bar{\omega} = \omega h\sqrt{\rho / G}$ of a simply supported nonlocal plate model ( $a = 10\,\text{nm}$, $E = 30\times10^6\ \text{Pa}$, $\nu = 0.3$ )

| $b/a$ | $a/h$ | $\mu$ | Classical | FSDT (Ref. [19]) | Present |
|---|---|---|---|---|---|
| 1 | 10 | 0 | 0.0963 | 0.0930 | **0.0930528** |
| | | 1 | 0.0880 | 0.0850 | **0.0850372** |
| | | 2 | 0.0816 | 0.0788 | **0.0787902** |
| | | 3 | 0.0763 | 0.0737 | **0.0737444** |
| | | 4 | 0.0720 | 0.0696 | **0.0695584** |
| | | 5 | 0.0683 | 0.0660 | **0.0660129** |
| | 20 | 0 | 0.0241 | 0.0239 | **0.0238705** |
| | | 1 | 0.0220 | 0.0218 | **0.0218143** |
| | | 2 | 0.0204 | 0.0202 | **0.0202118** |
| | | 3 | 0.0191 | 0.0189 | **0.0189174** |
| | | 4 | 0.0180 | 0.0178 | **0.0178436** |
| | | 5 | 0.0171 | 0.0169 | **0.0169340** |
| 2 | 10 | 0 | 0.0602 | 0.0589 | **0.0589024** |
| | | 1 | 0.0568 | 0.0556 | **0.0555738** |
| | | 2 | 0.0539 | 0.0527 | **0.0527525** |
| | | 3 | 0.0514 | 0.0503 | **0.0503213** |
| | | 4 | 0.0493 | 0.0482 | **0.0481980** |
| | | 5 | 0.0473 | 0.0463 | **0.0463227** |
| | 20 | 0 | 0.0150 | 0.0150 | **0.0149699** |
| | | 1 | 0.0142 | 0.0141 | **0.0141240** |
| | | 2 | 0.0135 | 0.0134 | **0.0134069** |
| | | 3 | 0.0129 | 0.0128 | **0.0127891** |
| | | 4 | 0.0123 | 0.0123 | **0.0122494** |
| | | 5 | 0.0118 | 0.0118 | **0.0117728** |

**Second case ($\mu_0 = \mu_1 = 0$):** The free vibration solution presented in Eq. (26) is numerically evaluated here for FG-CNTRC nanoplate to discuss the effects of nonlocal parameters on the plate vibration response. The presented formulations for GNSG plate model reduces to pure strain-gradient case. The nanoplate is fully simply-supported. The following mechanical properties for the polymer matrix are considered in this study:

$$a / b = 1 , E_m = 2.1\ GPa , v_m = 0.34 , \rho_m = 1.15\ gr / cm^3 \tag{39}$$

Fig. 2 displays the non-dimensional fundamental frequency $\bar{\omega}_c = \omega a^2 / h\sqrt{\rho_m / E_m}$ of a square nanoplate for different values of strain-gradient parameter ( $l / h$ ) and length to thickness ratios ( $a / h$ ). Fig. 2 illustrates exact agreement with the results obtained by (Shahriari et al. [55]).

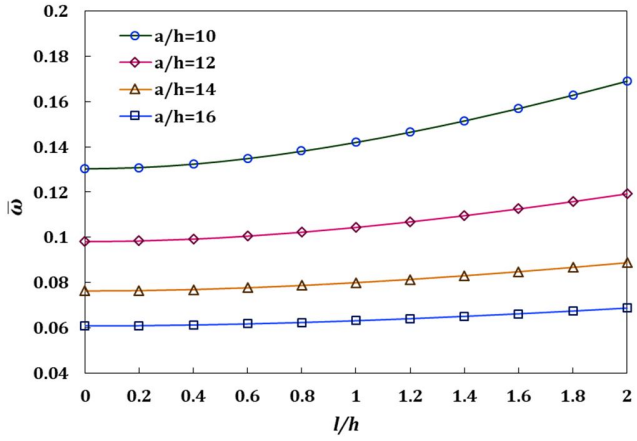


**Fig. 2** Non-dimensional fundamental frequency $\bar{\omega}_c = \omega a^2 / h\sqrt{\rho_m / E_m}$ presented model and Ref. [55]

In conclusion, the two validation cases show that the proposed model and solution procedure are able to predict the natural frequencies of nanoplates accurately.

### *6.1.2. Convergence of the method*

The convergence is studied by gradually increasing the number of polynomials used in each natural coordinate for the flexural and shear modes ($W, \Phi_x, \Phi_y$). To obtain reliable and comparatively accurate results, it is necessary to study convergence of the solution model. Fig. 3 shows the convergence of first three dimensionless natural frequencies for SSSS, CCCC and FFFF boundary conditions. It is clearly seen that convergence is achieved as we increase the number of polynomial terms. One may notice that $\mathrm{N} = 32$ is sufficient for computing the results.

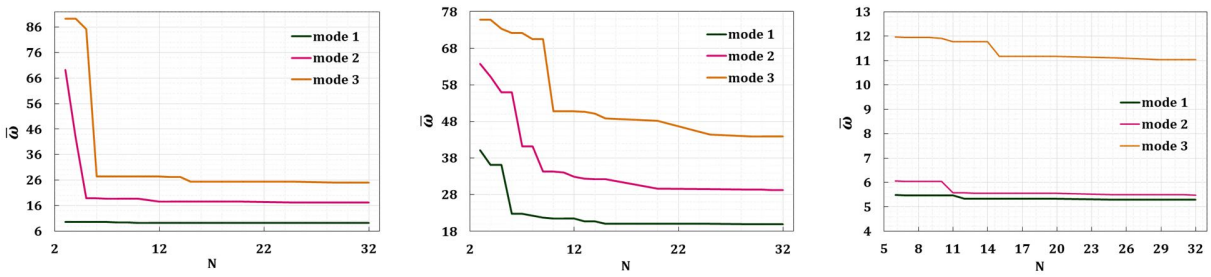


**Fig. 3** Convergence of first three natural frequencies for: **a)** SSSS, **b)** CCCC and **c)** FFFF boundary conditions

*6.1.3. Effect of thickness and aspect ratio in different theories*

In this subsection, the first two dimensionless natural frequencies of nanoplates $\bar{\omega}_c = \omega a^2 / h\sqrt{\rho / E_1}$ are studied based on different continuum theories such as classical plate theory ($\sqrt{\mu_0} = \sqrt{\mu_1} = l = 0$), pure nonlocal theory ($\sqrt{\mu_0} = 1\text{nm}, \sqrt{\mu_1} = l = 0$), pure strain-gradient theory ($\sqrt{\mu_0} = \sqrt{\mu_1} = 0, l = 1\text{nm}$), reduced nonlocal strain-gradient theory ($\sqrt{\mu} = l = 1\text{nm}$) and generalized nonlocal strain-gradient theory ($\sqrt{\mu_0} = \sqrt{\mu_1} = l = 1\text{nm}$). These results are provided in Table 4 by taking thickness ratio $h/b = \{0.02, 0.2\}$ and aspect ratio $a/b = \{1, 2\}$ for several possible boundary conditions. Here, the following parameters are used to obtain the numerical values:

$$a = 10\,,\ E_1 = 1.06\ \text{TPa}\ \ ,\nu = 0.3\,,\ \rho = 2250\ \text{kg}/\text{m}^3 \tag{40}$$

It is observed, that in the most cases by increasing $h/b$ and decreasing $a/b$ the frequency parameters $\bar{\omega}_c$ decrease. But in some cases with boundary conditions including free edges, an opposite behavior is seen (e.g., fundamental frequency of CFCF and SFSF nanoplates).

Fig. 4 shows the relative difference of other continuum theories (the classical, pure nonlocal, pure strain-gradient and reduced nonlocal strain-gradient theories) compared to GNSG theory for several possible boundary conditions, thickness and aspect ratios based on the data obtained from the Table 4. As mentioned before, the GNSG plate model is considered as a benchmark case in our analysis. The five theories (classical, pure nonlocal, pure strain-gradient, reduced nonlocal strain-gradient, generalized nonlocal strain-gradient) are compared. A discrepancy between the GNSG theory results and other theories is found in Table 4. This is obviously because the classical theory cannot exhibit the size-effects. Also the PSG and PNL theories have only a single length-scale coefficient and a nonlocal parameter, respectively; which both the theories are unable to capture the strain-gradients and nonlocalities in materials, simultaneously. Likewise, the results from RNSG and GNSG theories are different, which will be more discussed in section 6.1.5.

**Table 4.** Effects of thickness ratio $h/b$, aspect ratio $a/b$ and boundary conditions on the first two non-dimensional natural frequencies $\bar{\omega}_c = \omega a^2 / h\sqrt{\rho / E_1}$ for different continuum theories of plate.

| B.C. | a / b | h / b | Classical Theory | | PNL Theory | | PSG Theory | | RNSG Theory | | GNSG Theory | |
|---|---|---|---|---|---|---|---|---|---|---|---|---|
| | | | Mode1 | Mode2 | Mode1 | Mode2 | Mode1 | Mode2 | Mode1 | Mode2 | Mode1 | Mode2 |
| SSSS | 1 | 0.02 | 5.966 | 14.929 | 5.452 | 12.214 | 6.488 | 17.951 | 5.928 | 14.662 | 5.814 | 13.786 |
| | | 0.2 | 5.281 | 11.572 | 4.826 | 9.467 | 5.745 | 13.957 | 5.250 | 11.400 | 5.160 | 10.883 |
| | 2 | 0.02 | 14.925 | 23.909 | 12.213 | 17.870 | 17.214 | 31.266 | 14.074 | 23.331 | 12.647 | 21.533 |
| | | 0.2 | 13.768 | 21.158 | 11.266 | 15.814 | 15.951 | 27.685 | 13.039 | 20.658 | 11.823 | 19.230 |
| SFSF | 1 | 0.02 | 2.919 | 4.901 | 2.783 | 4.437 | 3.039 | 5.230 | 2.897 | 4.735 | 2.823 | 4.590 |
| | | 0.2 | 2.724 | 4.306 | 2.597 | 3.908 | 2.839 | 4.664 | 2.707 | 4.232 | 2.646 | 4.134 |
| | 2 | 0.02 | 2.880 | 8.336 | 2.746 | 6.630 | 3.002 | 8.978 | 2.863 | 7.136 | 2.796 | 6.496 |
| | | 0.2 | 2.826 | 7.625 | 2.695 | 6.102 | 2.949 | 8.485 | 2.812 | 6.784 | 2.747 | 6.228 |
| CFFF | 1 | 0.02 | 1.059 | 2.585 | 1.035 | 2.411 | 1.081 | 2.737 | 1.055 | 2.550 | 1.048 | 2.497 |
| | | 0.2 | 1.015 | 2.251 | 0.993 | 2.105 | 1.038 | 2.409 | 1.014 | 2.251 | 1.009 | 2.218 |
| | 2 | 0.02 | 1.056 | 4.511 | 1.032 | 3.674 | 1.079 | 4.882 | 1.054 | 3.973 | 1.047 | 3.637 |
| | | 0.2 | 1.031 | 4.082 | 1.007 | 3.346 | 1.059 | 4.537 | 1.035 | 3.717 | 1.031 | 3.432 |
| CFCF | 1 | 0.02 | 6.712 | 8.006 | 6.327 | 7.188 | 8.007 | 10.207 | 7.534 | 9.166 | 8.194 | 9.972 |
| | | 0.2 | 5.328 | 6.060 | 5.042 | 5.469 | 6.058 | 7.089 | 5.738 | 6.407 | 6.042 | 6.665 |
| | 2 | 0.02 | 6.698 | 10.934 | 6.315 | 8.639 | 7.989 | 14.142 | 7.517 | 11.178 | 8.166 | 11.580 |
| | | 0.2 | 6.232 | 9.473 | 5.882 | 7.545 | 7.327 | 12.018 | 6.911 | 9.570 | 7.431 | 9.753 |
| CCCC | 1 | 0.02 | 10.844 | 30.685 | 9.738 | 24.688 | 14.075 | 56.156 | 12.609 | 45.201 | 13.906 | 51.143 |
| | | 0.2 | 8.032 | 14.053 | 7.263 | 11.397 | 9.486 | 18.138 | 8.589 | 14.809 | 8.978 | 15.078 |
| | 2 | 0.02 | 29.705 | 74.463 | 23.423 | 54.207 | 50.577 | 184.462 | 39.664 | 134.397 | 42.976 | 151.710 |
| | | 0.2 | 23.300 | 29.520 | 18.578 | 21.574 | 33.729 | 45.799 | 27.127 | 33.859 | 28.467 | 34.952 |
| CCSS | 1 | 0.02 | 8.164 | 18.548 | 7.379 | 14.959 | 9.642 | 25.268 | 8.689 | 20.233 | 8.954 | 19.842 |
| | | 0.2 | 6.580 | 12.778 | 5.973 | 10.403 | 7.472 | 16.153 | 6.780 | 13.153 | 6.867 | 12.845 |
| | 2 | 0.02 | 21.485 | 31.231 | 17.157 | 22.706 | 29.476 | 47.884 | 23.283 | 34.522 | 22.126 | 32.935 |
| | | 0.2 | 18.300 | 25.158 | 14.716 | 18.532 | 23.881 | 36.391 | 19.158 | 26.762 | 18.384 | 25.708 |
| CFSF | 1 | 0.02 | 4.605 | 6.249 | 4.357 | 5.625 | 5.071 | 7.188 | 4.791 | 6.461 | 4.868 | 6.541 |
| | | 0.2 | 3.970 | 5.137 | 3.764 | 4.645 | 4.319 | 5.800 | 4.093 | 5.244 | 4.142 | 5.273 |
| | 2 | 0.02 | 4.573 | 9.489 | 4.327 | 7.520 | 5.041 | 11.112 | 4.763 | 8.790 | 4.843 | 8.455 |
| | | 0.2 | 4.373 | 8.514 | 4.140 | 6.793 | 4.813 | 10.061 | 4.552 | 8.019 | 4.626 | 7.736 |
| FFFF | 1 | 0.02 | 4.143 | 5.975 | 3.742 | 4.833 | 4.178 | 6.246 | 3.770 | 5.017 | 3.474 | 4.380 |
| | | 0.2 | 3.628 | 5.305 | 3.289 | 4.390 | 3.799 | 5.560 | 3.440 | 4.566 | 3.221 | 4.037 |
| | 2 | 0.02 | 6.559 | 8.138 | 5.319 | 6.475 | 6.935 | 8.306 | 5.577 | 6.596 | 4.866 | 5.680 |
| | | 0.2 | 6.324 | 7.445 | 5.165 | 5.960 | 6.695 | 7.900 | 5.420 | 6.313 | 4.748 | 5.492 |

It can be seen from Fig. 4 that boundary conditions significantly affect the solution. Also it is found that the differences among the plate theories are more prominent in the second mode of vibration. It means that the scale parameters have an essential role in the vibration analysis of nanoplates at higher modes. In some cases (e.g., CCCC and CFCF nanoplates) the results from the classical and RNSG theories are smaller than their counterparts from the GNSG theory. For the special case of FFFF nanoplate, the results based on PNL theory are larger than those from GNSG plate theory.

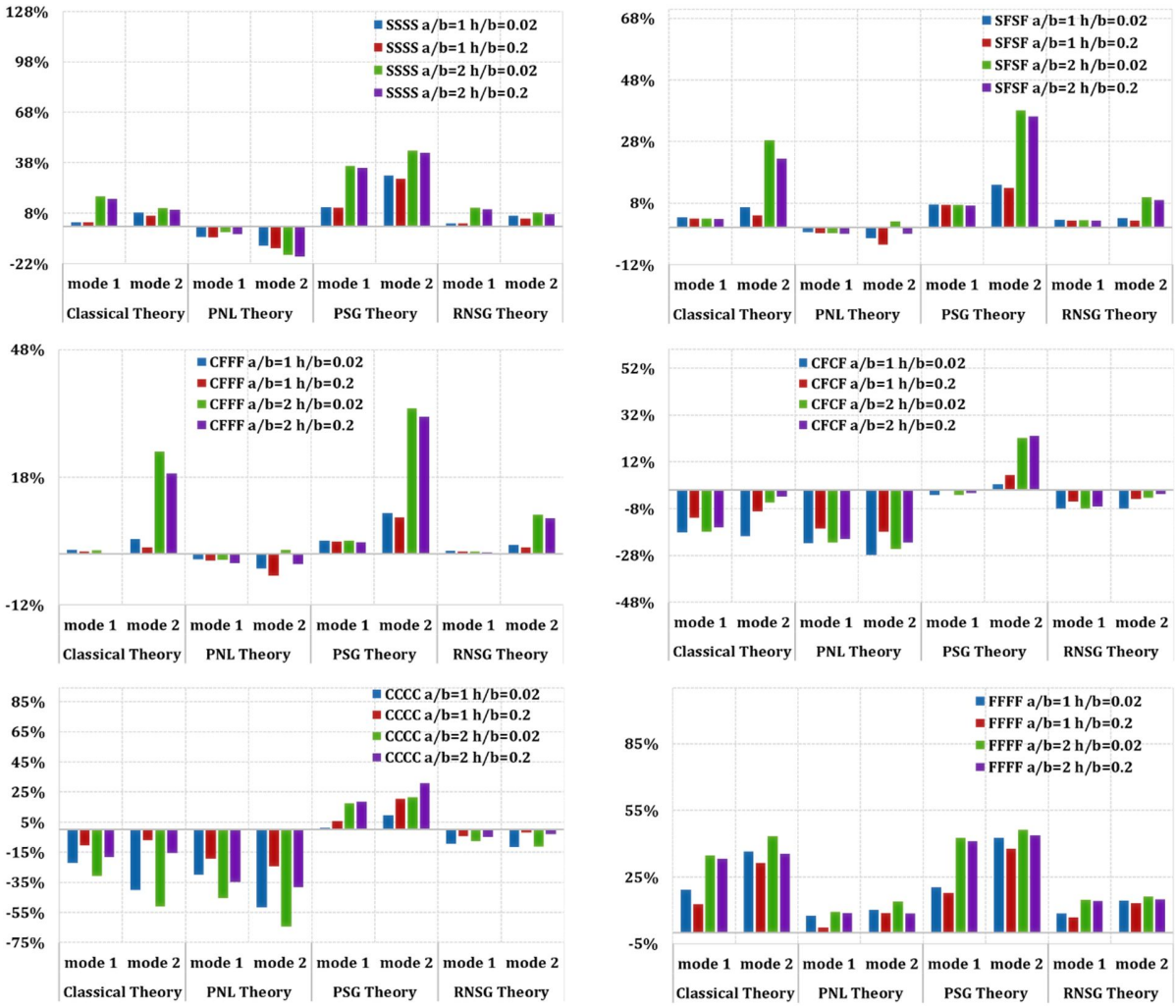


**Fig. 4** Relative difference of other continuum theories compared to GNSG theory for several possible boundary conditions, thickness and aspect ratios based on the data obtained from Table 4.

### *6.1.4. Effect of size-dependent parameters*

The variation of the first three dimensionless frequencies with nonlocal parameters ($\mu_0, \mu_1$) and strain-gradient parameter ($l$) has been demonstrated in Fig. 5 for a SSSS nanoplate based on the GNSG theory. Here the mechanical properties of the nanoplate are taken from Eq. (38). The first three modes of vibration are considered in this investigation. It is seen that frequency parameters increase with $l$ and decrease with $\mu_0$ and $\mu_1$. The effect of lower-order nonlocal parameter $\mu_0$ on the decrement of the frequency parameters $\bar{\omega}$ is more than that of the higher-order nonlocal parameter $\mu_1$, due to the fact that the location and mechanism of the two nonlocal parameters are induced in Eq. (6) differently. Here also, one may observe that effect of the nonlocal parameters ($\mu_0$, $\mu_1$) and strain-gradient parameter ($l$) on frequency parameters becomes more prominent in higher modes. Three cases studied in fig. 5 are listed as the following Equations:

$$\left[1-\mu_0\nabla^2\right]\mathrm{t}=\mathbb{C}:\epsilon-\left[1-\mu_0\nabla^2\right]l^2\nabla\cdot\mathbb{C}:\nabla\epsilon$$
$$\left[1-\mu_1\nabla^2\right]\mathrm{t}=\left[1-\mu_1\nabla^2\right]\mathbb{C}:\epsilon-l^2\nabla\cdot\mathbb{C}:\nabla\epsilon \qquad (41)$$
$$\left[1-\mu_1\nabla^2\right]\left[1-\mu_0\nabla^2\right]\mathrm{t}=\left[1-\mu_1\nabla^2\right]\mathbb{C}:\epsilon$$

By Substituting $\mu_1=0$, $\mu_0=0$ and $l=0$ into the Eq. (6), the equations (41), (42) and (43) can be obtained, which belong to the three cases depicted in Fig. (5-a,d,g), Fig. (5-b,e,h) and Fig. (5-c,f,i), respectively.

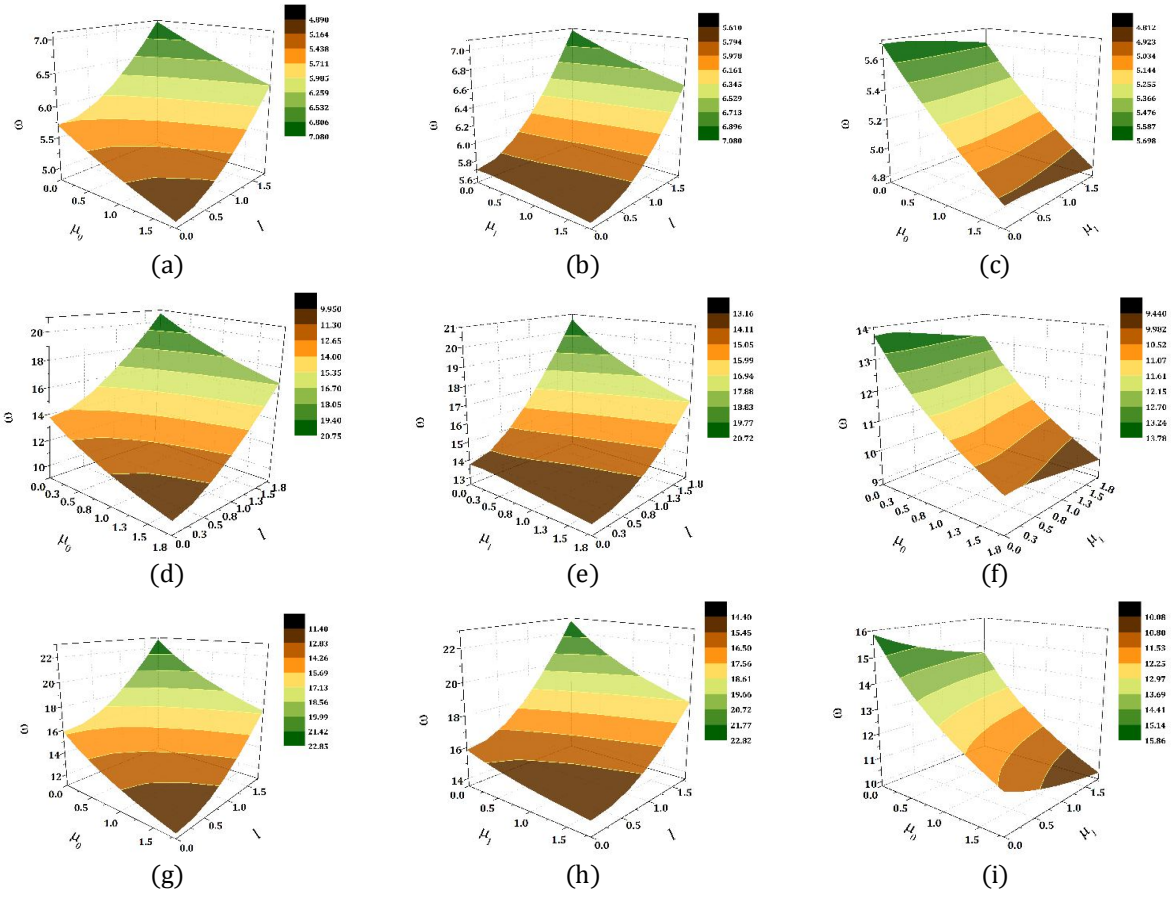


**Fig. 5** Variation of the: **(a-c)** First, **(d-f)** Second and **(g-i)** Third non-dimensional frequencies with nonlocal parameters ( $\mu_0$ , $\mu_1$ ) and strain-gradient length scale parameter ( $l$ )

### *6.1.5. Simplification of GNSG model (RNSG vs. GNSG)*

In the Figs. 6-8, the variation of first three frequency parameters of the two RNSG and GNSG theories is compared by changing the parameters $l$ and $\mu_0=\mu_1=\mu$ for a fully simply-supported

nanoplate. The mechanical properties are taken from Eq. (38). The variation of relative error percentage arises between the two models is also depicted for each vibration mode.

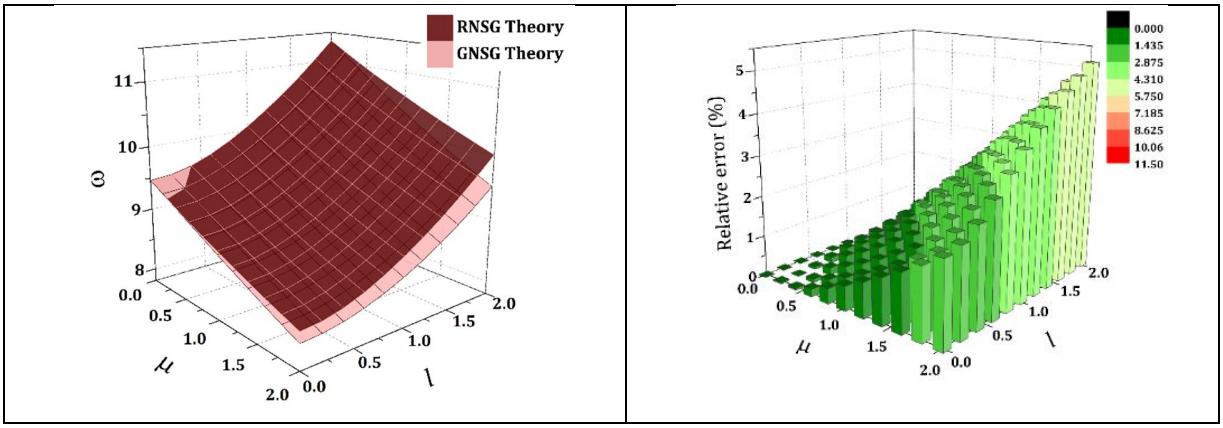


(a) (b)

**Fig. 6 a)** Variation of the first mode non-dimensional frequency of the RNSG and GNSG theories with ( $\mu_0 = \mu_1 = \mu$ ) and $l$ , **b)** Relative error percentage between the two models for each point ( $\mu, l$ )

It is observed that for the higher modes the relative error percentage is increased. It means that the simplification of the GNSG theory to the RNSG theory is not acceptable especially for higher modes. It's worth stressing that most researchers applied only the reduced nonlocal strain-gradient theory in their analysis, which neglects the higher order gradients (Li and Hu [41], Li and Hu[43], Li *et al*. [45], Li *et al*.[46], Ebrahimi *et al*.[47]).

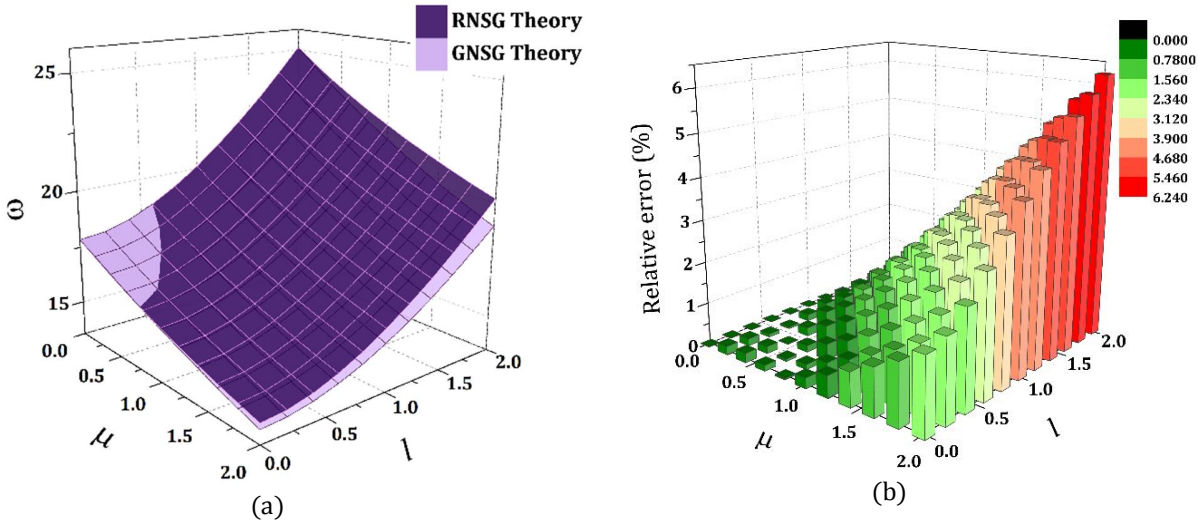


(a) (b)

**Fig. 7 a)** Variation of the second mode non-dimensional frequency of the RNSG and GNSG theories with ( $\mu_0 = \mu_1 = \mu$ ) and $l$ , **b)** Relative error percentage arises between the two models for each point ( $\mu, l$ )

From Figs. 6-8 we may also observe that the relative error percentage is increased with increasing each parameters $\mu$ and $l$ for all vibration modes. For example, in the fig. 6, 7 and 8 the maximum relative error percentage equals to 5.12%, 6.23% and 17.78% for the first, second

and third modes, respectively. We also can realize that within a limited domain (for small values of $\mu$ and $l$), the results from GNSG theory become a bit larger than those of RNSG theory.

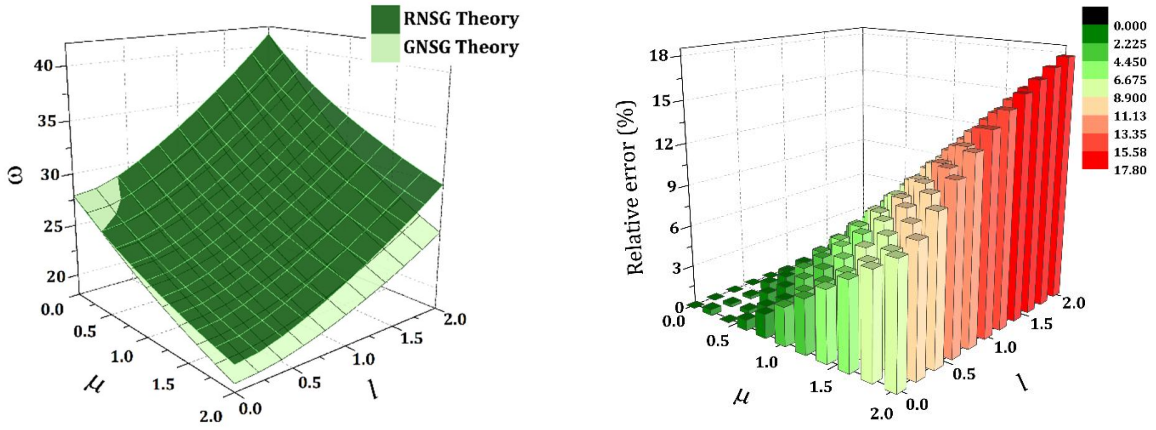


(a) (b)

**Fig. 8 a)** Variation of the third mode non-dimensional frequency of the RNSG and GNSG theories with ( $\mu_0 = \mu_1 = \mu$ ) and $l$ , **b)** Relative error percentage arises between the two models for each point ( $\mu, l$ )

### *6.1.6. Effect of aspect ratio*

Figs. 9-12 present the variation of the first four dimensionless frequencies with aspect ratio based on different continuum theories for a SSSS, CFFF, SFSF and CFCF nanoplate. We have used the material properties of the Equation (40) in our analysis in Figs. (9-12). The scale parameters are considered as: $\mu_0 = \mu_1 = 1\,\text{nm}^2$ and $l = 1\,\text{nm}$ . The figures show that the frequency parameters increase with aspect ratio and the effect of the aspect ratio becomes more noticeable in the higher vibration modes. It is also observed that unlike the most cases, in some boundary conditions the frequency parameter curve computed based on GNSG theory is plotted on the top of the curves of the PSG/Classical theories (e.g. in the fig. 12 in the first mode).

As the length ( $a$ ) of the nanoplate increases ( $b = \text{constant}$), the dimension of the plate is being larger along $x-$ direction and thus, the softening effect of the nonlocal parameters ( $\mu_0, \mu_1$ ) is vanishing gradually. This is in agreement with other reports in the literature where increasing any dimension of a structure decreases the influence of scale parameters and the model reverts to an equivalent classical-local model. In the Fig. 10 and 11, the fundamental and second mode frequencies will be fixed after a special value of aspect ratio for the classical and PSG theories. This "fixing phenomenon" is occurred duo to the fact that after a range of aspect ratios, when $a/b$ increases, the frequency curves get close to the frequencies of the fundamental and first over-tone modes of a classical-local cantilever beam. Thus, in this case we have a narrow and long plate. This time, for the other cases (PNL, RNSG and GNSG theories), the effect of nonlocal parameters is the cause of a shift in fixing the frequencies after specific range of aspect ratio. For the classical plate and PSG plate this phenomenon happens faster than other theories. For the PSG plate model, the strain-gradient parameter actually does affect the structural stiffness and pushes the cusp point of the fixing phenomenon further than classical one.

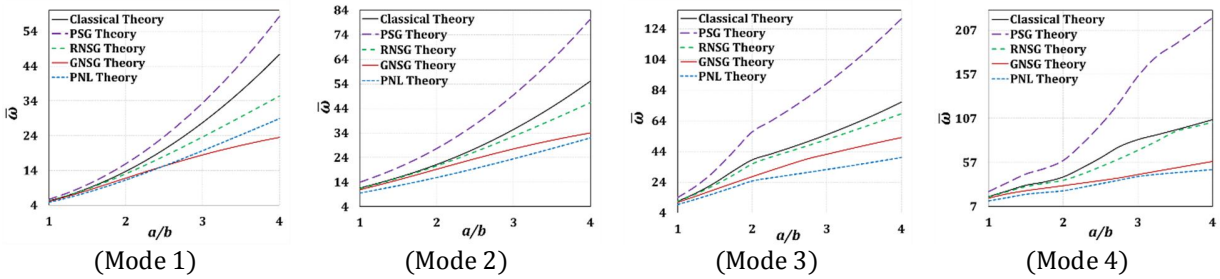


**Fig. 9** Variation of first four dimensionless frequencies of a SSSS nanoplate with aspect ratio for different continuum theories

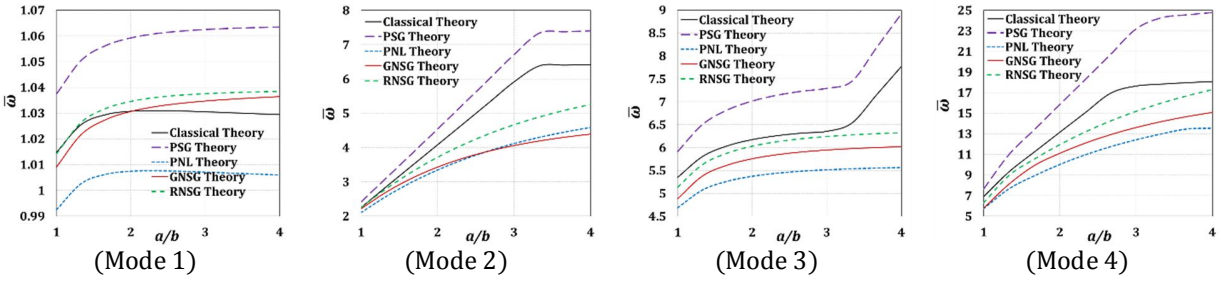


**Fig. 10** Variation of first four dimensionless frequencies of a CFFF nanoplate with aspect ratio for different continuum theories

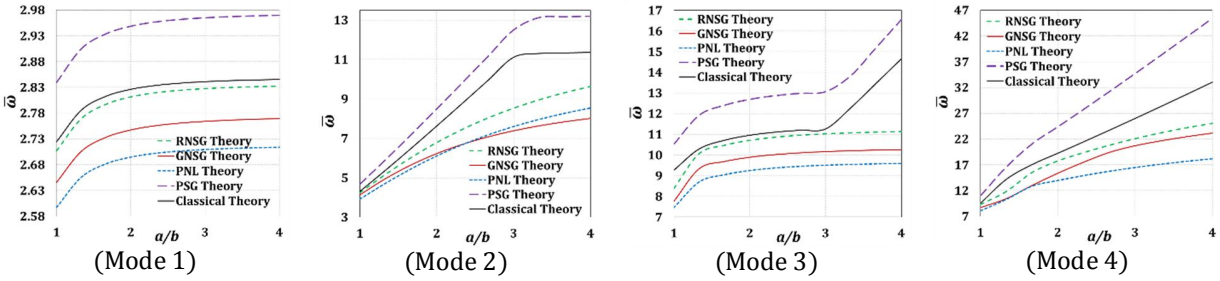


**Fig. 11** Variation of first four dimensionless frequencies of a SFSF nanoplate with aspect ratio for different continuum theories

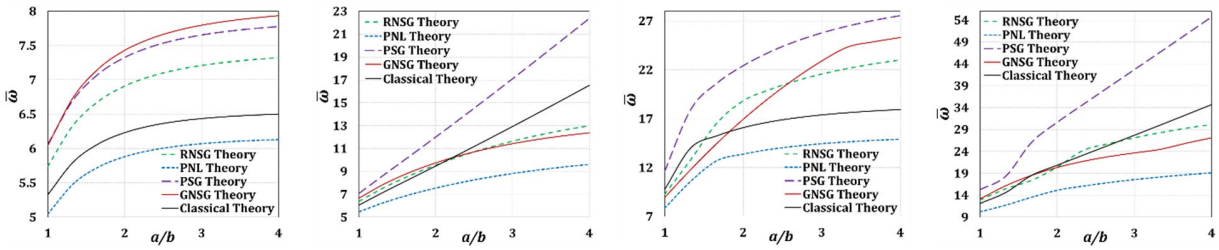


**Fig. 12** Variation of first four dimensionless frequencies of a CFCF nanoplate with aspect ratio for different continuum theories

## *6.2. Wave propagation analysis*

To explain the size effects of the generalized nonlocal strain-gradient theory for wave propagation in materials at nano-scales, some numerical examples are presented and discussed. First, to test the applicability of the present size-dependent plate theory for wave propagation in graphene sheets, the flexural dispersion curve for a single-layer graphene is obtained using the GNSG plate model and compared with experimental results in Fig. 13. The nonlocal parameters and strain-gradient parameter are determined by fitting flexural dispersion function to experimental data (Mohr *et al.*[56]): $\mu_0=\mu_1=0.00371\times10^{-18}\ \text{nm}^2$, $l=9.09615\times10^{-12}\ \text{nm}$. The material properties of the orthotropic plate model are taken from the elastic properties ( $h=0.129\,\text{nm}$, $E_1=2434\,\text{GPa}$, $E_2=2473\,\text{GPa}$, $G_{12}=G_{13}=G_{23}=1039\,\text{GPa}$, $\nu_{12}=\nu_{21}=0.197$, $\rho$=6316kg/m$^3$ ) of a specific single-layer graphene presented by Shen *et al.*[57]. It is assumed that wave propagates only along $x-$ direction ($k_y=0, k_x=k$) in an armchair graphene sheet (see, Fig. 1 for details).

Fig. 13 shows dispersion curve based on the classical-local plate theory, which fails to capture the stiffness adjustment effect of the scale parameters and over-predicts the frequencies. Unlike the classical-local plate model, the calculated results from GNSG plate model are perfectly in good agreement with experimental data. Therefore the present GNSG plate model can be applicable for simulating wave propagation phenomenon in graphene sheets.

From now on, the nanoplate under investigation is considered as homogeneous and isotropic with the following geometric and mechanical properties: $a=10\,\text{nm}$, $h=2\,\text{nm}$, $E=1.06\,\text{TPa}$, $\nu=0.3$, $\rho=2250\,\text{kg/m}^3$ and $K_s=5/6$ (Shear correction factor). The dispersion relation between the wave frequency parameter ($\bar{\omega}=\omega h\sqrt{\rho_0/G}$) and the dimensionless wavenumber ($\bar{K}=kh$) for various non-dimensional nonlocal parameters ($\theta_0=\sqrt{\mu_0}/h$, $\theta_1=\sqrt{\mu_1}/h$) and dimensionless strain-gradient parameter ($\beta=l/h$) are illustrated in Fig. 14. In this figure, the wave frequencies increase continuously with increasing $\bar{K}$ in general, but with different rates. The wave propagation solution for the CLT theory without scale effects can be deduced by taking $\theta_0$, $\theta_1$ and $\beta$ to zero. In this case, for higher values of $\bar{K}$, the wave frequency varies linearly and the wave propagates non-dispersively. For the cases when $l$ is dominant ($\{\theta_0=1/8,\theta_1=1/4,\beta=1/2\}$, $\{\theta_0=1/4,\theta_1=1/8,\beta=1/2\}$), the dispersion curves appear between CPT and PSG curves. On the

other hand, the dispersion relation tends to be dispersive for dominant nonlocal parameters ({ $\theta_0 = 1/2, \theta_1 = 1/4, \beta = 1/8$ }, { $\theta_0 = 1/4, \theta_1 = 1/2, \beta = 1/8$ }).

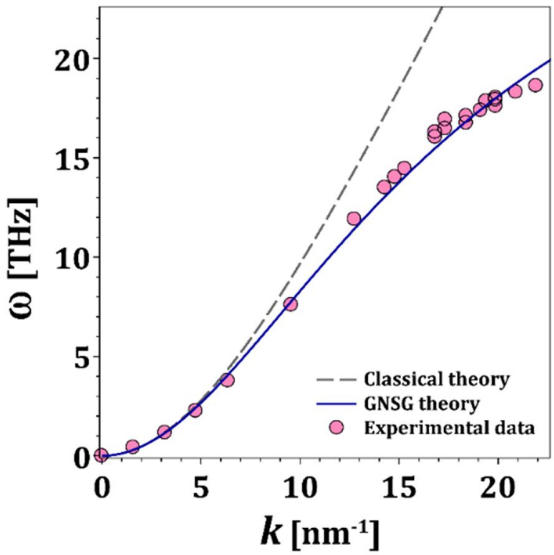


**Fig. 13** Flexural dispersion curves of a single-layer graphene from experimental data (Mohr et al. [56]) compared with GNSG and classical plate models ( $\mu_0 = \mu_1 = 0.00371 \times 10^{-18}$ nm$^2$, $l = 9.09615 \times 10^{-12}$ nm ).

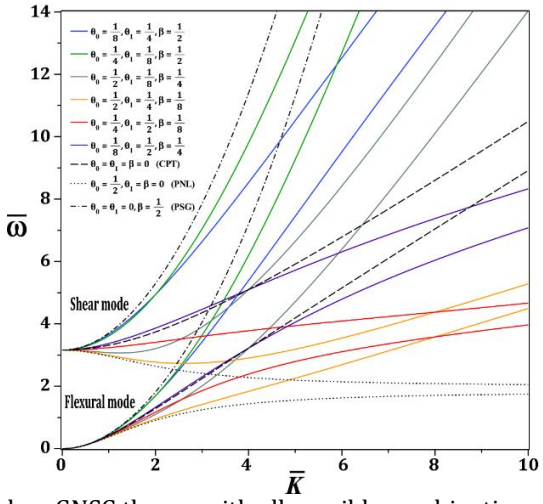


**Fig. 14** Dispersion curves based on GNSG theory with all possible combinations of dimensionless nonlocal and strain-gradient parameters. The other theories (CLT, PNL, PSG) are demonstrated with the black lines.

In a special case $(\theta_0 = 1/8, \theta_1 = 1/2, \beta = 1/4)$, it is noticed that with increasing $\bar{K}$, $\bar{\omega}$ becomes slightly higher than the classical solution in a range of wavenumbers ($\bar{K} \le 4$) while as $\bar{K}$ further increases ($\bar{K} > 4$), $\bar{\omega}$ becomes lower than the classical solution. In another special case (

$(\theta_0 = 1/2, \theta_1 = 1/8, \beta = 1/4)$), this trend is completely inverse. These particular cases originated from both the diminution and enhancement effects of the new higher-order generalized nonlocal strain-gradient plate model.

The influence of the nonlocal parameters and strain-gradient parameter on dispersion relations is further illustrated in Figs. 15-18. Here the non-dimensional nonlocal and strain-gradient parameters are taken from the Table 5:

**Table 5.** Different continuum theories considered in figs. 15-18.

| Continuum theory | $\theta_0$ | $\theta_1$ | $\beta$ |
|---|---|---|---|
| CLT | 0 | 0 | 0 |
| PNL | 1/2 | 0 | 0 |
| PSG | 0 | 0 | 1/4 |
| GNSG | 1/2 | 1/2 | 1/4 |

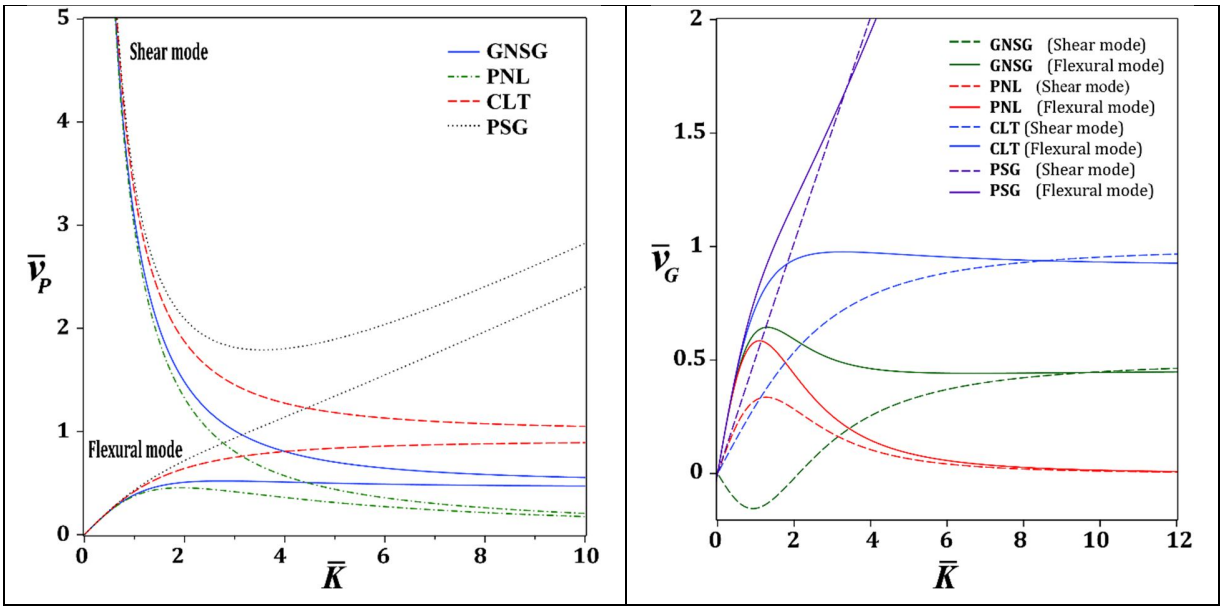


(a) (b)

**Fig. 15** Comparison of the a) Phase velocity and b) Group velocity dispersions in nanoplates modeled by several continuum theories

From Fig. 15-a it can be seen that there are two wave mode branches (flexural and shear). The figure shows the dimensionless phase velocity $\bar{v}_P$ as a function of $\bar{K}$. For both flexural and shear mode branches, the wave phase velocities of all the plate continuum models (GNSG, PNL, CLT and PSG) are very close to each other and non-dispersive for small values of dimensionless wavenumber ($\bar{K} < 0.7$). However, for the flexural mode branch, the phase velocity increases gradually with increasing $\bar{K}$ for the CLT model, while it increases sharply for the PSG model. For the PNL model, the phase velocity decreases continuously with $\bar{K}$ but for the GNSG model, the stiffness enhances due to the presence of the strain-gradient

parameter ($\beta$), which makes the GNSG curve appear above the PNL curve. This time for the shear mode branch, the phase velocity drops sharply for small values of $\bar{K} < 3.8$ for all the continuum theories. In this case, as $\bar{K}$ further increases ($\bar{K} > 3.8$), the phase velocity decreases more slightly and converges to the flexural mode curve for each plate model. At very large wavenumbers ($\bar{K} \to \infty$), it is expected that $\bar{v}_P$ tends to zero for the PNL model due to presence of the escape frequency. A very sharp increase in PSG curve can be observed for $\bar{K} > 3.8$ because of the strain-gradient stiffening effect.

The fig. 15-b shows the dimensionless group velocity $\bar{v}_G$ as a function of $\bar{K}$. The shear mode curves are shown with dashed lines. For flexural modes it is observed that the lowest curve belongs to the PNL model due to the fact that nonlocal parameter introduces the escape frequency where the group velocity tends to zero. The highest curve above the others belongs to the PSG theory. The GNSG curve is limited between the PNL and CLT curves only for flexural mode. In the shear mode, all of the theories demonstrate a non-dispersive linear behavior for small values of $\bar{K} < 0.7$ but as the wavenumber increases, the PNL, CLT and GNSG curves become dispersive and nonlinear excluding the PSG model, which for all values of $\bar{K}$ its curve shows a linear (non-dispersive) relationship between $\bar{K}$ and $\bar{v}_G$. It is worth noting that the PSG curve monotonically increasing with $\bar{K}$ but for the CLT and PNL models the group velocity first increase sharply with small values of $\bar{K}$ and then slowly decreases asymptotically. There is an exceptional case of GNSG that shows a quite opposite behavior among the other theories for the shear mode; that is, with increasing $\bar{K}$ the curve first decreases (i.e., group velocity becomes negative and wave envelopes move in opposite direction) for small values of wavenumber ($\bar{K} < 1$) then increases for larger values of $\bar{K}$.

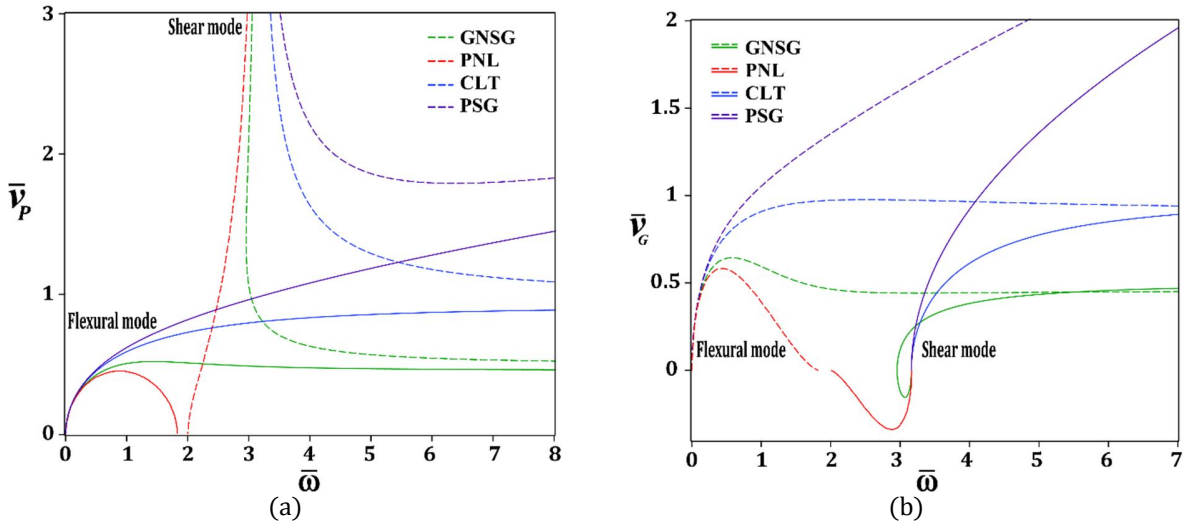


**Fig. 16** Comparison of the velocity- frequency **a)** $\bar{v}_P - \bar{\omega}$ and **b)** $\bar{v}_G - \bar{\omega}$ dispersion curves in nanoplates modeled by several continuum theories

Fig. 16 presents the dimensionless phase velocity ($\bar{v}_P$) and group velocity ($\bar{v}_G$) as a function of $\bar{\omega}$ for both flexural and shear wave modes. Generally, by increasing $\bar{\omega}$, the curves of the shear branch gradually approach their counterparts in flexural branch. In the fig. 16-a, the PSG curve

increases with increasing the dimensionless wave frequency ($\bar{\omega}$) for flexural modes but the PNL curve first increases for small value frequencies and then decreases due to the existence of the escape frequency originated from non-dimensional nonlocal parameter $\theta_0 = 1/2$ (i. e, an arc-type shape). It should be noted that in the PNL as $\theta_0$ tends to 1, the corresponding escape frequency decreases. The GNSG curve increases with small values of $\bar{\omega}$ and with further increase of $\bar{\omega}$ it imperceptibly decreases asymptotically and then it fixed. Thus unlike the PNL model the GNSG curve does not reach to zero. The GNSG phase velocity curve is appeared between the two PNL and CLT curves. In the shear modes, except the PNL case, which strongly increases with $\bar{\omega}$, the other theories decrease asymptotically.

In the fig. 16-b the PSG group velocity curve increases monotonically with $\bar{\omega}$ for both flexural and shear modes. Again close to the escape frequency the PNL curve tends to zero in flexural mode. The flexural curve of the GNSG model first increases with $\bar{\omega}$ then after a peak point it decreases slightly but it is not tends to zero as the PNL curve because of stiffness enhancement effect in GNSG model. In fact, the considered GNSG plate model have not an escape frequency. In the shear modes, the PNL curve is completely negative but the GNSG curve goes negative partly and then after increasing $\bar{\omega}$ enough, it then increases and becomes positive completely. The dispersion curve of the CLT group velocity increases with all values of wave frequencies $\bar{\omega}$ in the examined range but for larger $\bar{\omega}$ it will be reached to a fixed value.

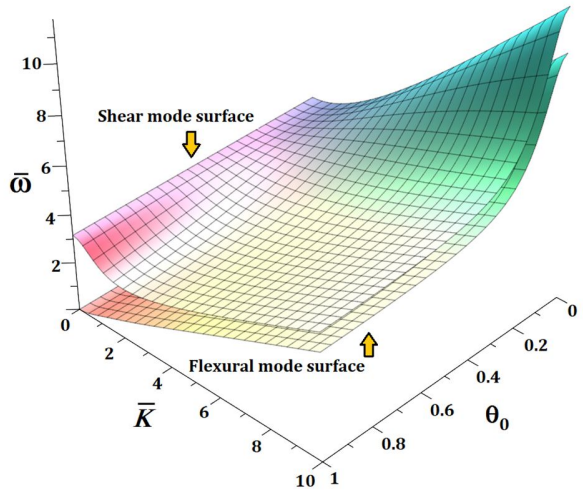


**Fig. 17** Effect of dimensionless nonlocal parameter $\theta_0$ on dispersion relation of a GNSG plate model

The influence of dimensionless nonlocal parameter $\theta_0$ on dispersion relation of a nanoplate based on GNSG theory is depicted for both flexural and shear modes in fig. 17. The material properties of the nanoplate is taken from Eq. (40) and $h = 2\,\mathrm{nm}$. The parameter $\theta_0$ varies from 0 to 1 and the non-dimensional scale parameters are taken as $\theta_1 = 1/2$ and $\beta = 1/4$. The fig. 17 shows the dimensionless wave frequency as a function of two variables as $\bar{\omega} = \bar{\omega}\left(\bar{K}, \theta_0\right)$. It can be seen that for both flexural and shear modes the wave frequency inversely proportional to $\theta_0$ but the effect of $\theta_0$ on the decrement of the $\bar{\omega}$ is more prominent in higher wavenumbers and it is insignificant for small values of $\bar{K} < 0.3$.

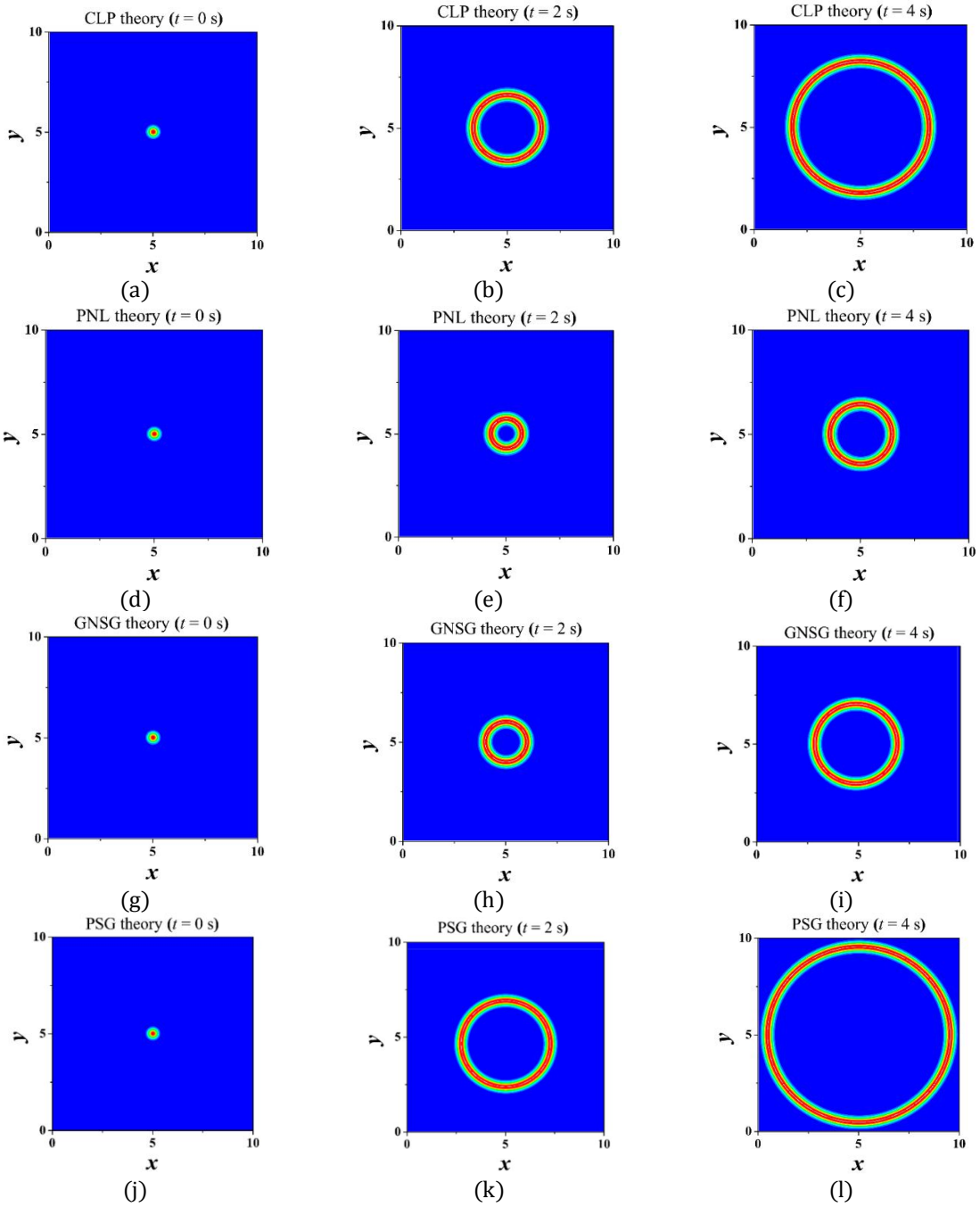


**Fig. 18** Fronts of the flexural solitary waves propagating through a square nanoplate modeled based on the (a-c) CLT theory, (d-f) PNL theory, (g-i) GNSG theory and (j-l) PSG theory. ( $a = 10$ , $k_x = k_y = 2\,\mathrm{nm}^{-1}$ , $h = 2$ )

Fig. 18 shows a traveling solitary wave propagating through a first-order shear deformation nanoplate with length $a = 10\,\mathrm{nm}$ at times $t = 0\,\mathrm{s}$ , $2\,\mathrm{s}$ and $4\,\mathrm{s}$ for classical elasticity, PNL elasticity , PSG theory and a general case of the present GNSG model (the nonlocal and strain-gradient parameters are taken from Table 5).

The wave fronts of all the four cases are adjusted by the wavenumber taken as ($k_x = k_y = 2\text{nm}^{-1}$) and starting to propagate from the source point at the middle of the nanoplate while $t = 0\,s$. From the fig. 18 it is apparent that the waves fronts are different in speed of propagation (propagation delays and advances) for different continuum theories due to the fact that the wave frequency and the speed of wave propagation is strongly influenced by the nonlocal and strain-gradient parameters ($\theta_0$, $\theta_1$ and $\beta$) included in the studied plate models. In this case, the speed of traveling flexural waves for the different continum theories are compared as below:

$$\text{PNL} < \text{GNSG} < \text{CLP} < \text{PSG} \tag{42}$$

This comparison of the waves speed in Eq. (44) is not always true and it depends on the value of the wavenumbers $k_x$ and $k_y$ and the chosen size-dependent parameters $\theta_0$, $\theta_1$ and $\beta$ in the problem.

## 7. Conclusions

To integrate the effects of higher-order nonlocal stress field with the nonlocal effects of strain-gradient stresses in a unified plate theory, a new size-dependent thick plate model is developed in this study. Two nonlocal parameters and a strain-gradient parameter are introduced to capture the size effects in the present plate model. Both increase and decrease in the stiffness of the nanoplates is feasible to happen depending on the values of these parameters. The free vibration and wave propagation of the first-order shear deformation nanoplate are calculated based on the generalized nonlocal strain-gradient theory. To predict the natural frequencies for different boundary conditions, an orthogonal polynomial-based Ritz method is employed. A closed-form of dispersion relation between the wave frequency (or phase/group velocity) and the wavenumber is obtained. An intensive parametric study is presented on the effects of nonlocal parameters, strain-gradient parameter, aspect and thickness ratios and boundary conditions on the natural frequencies and wave propagation. An error analysis conducted on the RNSG and GNSG plate theories and a divergence of results is estimated between the two models. The distinctive, progressively varying stiffness of nanoplates is not consistent with the pure nonlocal theory or the pure strain-gradient theory. This fact is true not only for free vibration analysis but also for the dispersion relations. On this basis, this new model predicts a stiffness enhancement effect for a range of wave-lengths with the presence of the nonlocal strain-gradients and this is quite different from the prevalent nonlocal stress-gradient models. The classical-local and PSG plate models generally overestimate the frequencies. Also the frequencies are underestimated by the PNL theory. As a result, the GNSG theory should be considered in the free vibration and wave propagation of nanoplates and the applicability of the proposed plate model is inevitable in this research.

## References

[1] J.A. Ruud, T.R. Jervis, F. Spaepen, Nanoindentation of Ag/Ni multilayered thin films, Journal of Applied Physics, 75 (1994) 4969-4974.

[2] P. Ball, Roll up for the revolution, Nature, 414 (2001) 142-144.
[3] R.H. Baughman, A.A. Zakhidov, W.A. De Heer, Carbon nanotubes--the route toward applications, science, 297 (2002) 787-792.
[4] B.H. Bodily, C.T. Sun, Structural and equivalent continuum properties of single-walled carbon nanotubes, International Journal of Materials and Product Technology, 18 (2003) 381-397.
[5] C. Li, T.W. Chou, A structural mechanics approach for the analysis of carbon nanotubes, International Journal of Solids and Structures, 40 (2003) 2487-2499.
[6] R. Liu, L. Wang, Thermal vibration of a single-walled carbon nanotube predicted by semiquantum molecular dynamics, Physical Chemistry Chemical Physics, 17 (2015) 5194-5201.
[7] G. Shi, P. Zhao, A new molecular structural mechanics model for the flexural analysis of monolayer graphene, Computer Modeling in Engineering & Sciences(CMES), 71 (2011) 67-92.
[8] P.L. De Andres, F. Guinea, M.I. Katsnelson, Density functional theory analysis of flexural modes, elastic constants, and corrugations in strained graphene, Physical Review B, 86 (2012) 245409.
[9] A.C. Eringen, Nonlocal polar elastic continua, International journal of engineering science, 10 (1972) 1-16.
[10] A.C. Eringen, On differential equations of nonlocal elasticity and solutions of screw dislocation and surface waves, Journal of applied physics, 54 (1983) 4703-4710.
[11] A.C. Eringen, Nonlocal continuum field theories, Springer Science & Business Media, 2002.
[12] W.H. Duan, C.M. Wang, Y.Y. Zhang, Calibration of nonlocal scaling effect parameter for free vibration of carbon nanotubes by molecular dynamics, Journal of applied physics, 101 (2007) 024305.
[13] Q. Wang, Q.K. Han, B.C. Wen, Estimate of material property of carbon nanotubes via nonlocal elasticity, Advanced Theoretical Applied Mechanics, 1 (2008) 1-10.
[14] L.Y. Huang, Q. Han, Y.J. Liang, Calibration of nonlocal scale effect parameter for bending single-layered graphene sheet under molecular dynamics, Nano, 7 (2012) 1250033.
[15] Y. Liang, Q. Han, Prediction of nonlocal scale parameter for carbon nanotubes, Science China Physics, Mechanics and Astronomy, 55 (2012) 1670-1678.
[16] A.A. Pisano, A. Sofi, P. Fuschi, Nonlocal integral elasticity: 2D finite element based solutions, International Journal of Solids and Structures, 46 (2009) 3836-3849.
[17] W.H. Duan, C.M. Wang, Exact solutions for axisymmetric bending of micro/nanoscale circular plates based on nonlocal plate theory, Nanotechnology, 18 (2007) 385704.
[18] P. Lu, P.Q. Zhang, H.P. Lee, C.M. Wang, J.N. Reddy, Non-local elastic plate theories, in: Proceedings of the royal society of london a: Mathematical, physical and engineering sciences, The Royal Society, 2007, pp. 3225-3240.
[19] R. Aghababaei, J.N. Reddy, Nonlocal third-order shear deformation plate theory with application to bending and vibration of plates, Journal of Sound and Vibration, 326 (2009) 277-289.
[20] H.T. Thai, A nonlocal beam theory for bending, buckling, and vibration of nanobeams, International Journal of Engineering Science, 52 (2012) 56-64.
[21] T. Murmu, S.C. Pradhan, Small-scale effect on the free in-plane vibration of nanoplates by nonlocal continuum model, Physica E: Low-dimensional Systems and Nanostructures, 41 (2009) 1628-1633.
[22] S. Faroughi, S.M.H. Goushegir, Free in-plane vibration of heterogeneous nanoplates using Ritz method, Journal of Theoretical and Applied Vibration and Acoustics, 2 (2016) 1-20.
[23] Y.Z. Wang, F.M. Li, K. Kishimoto, Flexural wave propagation in double-layered nanoplates with small scale effects, Journal of Applied Physics, 108 (2010) 064519.
[24] L. Wang, H. Hu, Flexural wave propagation in single-walled carbon nanotubes, Physical Review B, 71 (2005) 195412.
[25] B.o. Wang, Z. Deng, H. Ouyang, J. Zhou, Wave propagation analysis in nonlinear curved single-walled carbon nanotubes based on nonlocal elasticity theory, Physica E: Low-dimensional Systems and Nanostructures, 66 (2015) 283-292.
[26] M.A. Eltaher, M.A. Hamed, A.M. Sadoun, A. Mansour, Mechanical analysis of higher order gradient nanobeams, Applied Mathematics and Computation, 229 (2014) 260-272.
[27] C.W. Lim, G. Zhang, J.N. Reddy, A higher-order nonlocal elasticity and strain gradient theory and its applications in wave propagation, Journal of the Mechanics and Physics of Solids, 78 (2015) 298-313.
[28] H.M. Ma, X.L. Gao, J.N. Reddy, A microstructure-dependent Timoshenko beam model based on a modified couple stress theory, Journal of the Mechanics and Physics of Solids, 56 (2008) 3379-3391.
[29] N. Challamel, C.M. Wang, The small length scale effect for a non-local cantilever beam: a paradox solved, Nanotechnology, 19 (2008) 345703.

[30] N. Challamel, Z. Zhang, C.M. Wang, J.N. Reddy, Q. Wang, T. Michelitsch, B. Collet, On nonconservativeness of Eringen's nonlocal elasticity in beam mechanics: correction from a discrete-based approach, Archive of Applied Mechanics, 84 (2014) 1275-1292.
[31] C.M. Wang, S. Kitipornchai, C.W. Lim, M. Eisenberger, Beam bending solutions based on nonlocal Timoshenko beam theory, Journal of Engineering Mechanics, 134 (2008) 475-481.
[32] D.C.C. Lam, F. Yang, A.C.M. Chong, J. Wang, P. Tong, Experiments and theory in strain gradient elasticity, Journal of the Mechanics and Physics of Solids, 51 (2003) 1477-1508.
[33] E.C. Aifantis, On the role of gradients in the localization of deformation and fracture, International Journal of Engineering Science, 30 (1992) 1279-1299.
[34] F.A.C.M. Yang, A.C.M. Chong, D.C.C. Lam, P. Tong, Couple stress based strain gradient theory for elasticity, International Journal of Solids and Structures, 39 (2002) 2731-2743.
[35] J.N. Reddy, Microstructure-dependent couple stress theories of functionally graded beams, Journal of the Mechanics and Physics of Solids, 59 (2011) 2382-2399.
[36] H. Askes, E.C. Aifantis, Gradient elasticity and flexural wave dispersion in carbon nanotubes, Physical Review B, 80 (2009) 195412.
[37] B. Akgöz, Ö. Civalek, Application of strain gradient elasticity theory for buckling analysis of protein microtubules, Current Applied Physics, 11 (2011) 1133-1138.
[38] W. Xu, L. Wang, J. Jiang, Strain gradient finite element analysis on the vibration of double-layered graphene sheets, International Journal of Computational Methods, 13 (2016) 1650011.
[39] H.X. Nguyen, T.N. Nguyen, M. Abdel-Wahab, S.P.A. Bordas, H. Nguyen-Xuan, T.P. Vo, A refined quasi-3D isogeometric analysis for functionally graded microplates based on the modified couple stress theory, Computer Methods in Applied Mechanics and Engineering, 313 (2017) 904-940.
[40] Y.S. Li, E. Pan, Static bending and free vibration of a functionally graded piezoelectric microplate based on the modified couple-stress theory, International Journal of Engineering Science, 97 (2015) 40-59.
[41] L.i. Li, Y. Hu, Wave propagation in fluid-conveying viscoelastic carbon nanotubes based on nonlocal strain gradient theory, Computational materials science, 112 (2016) 282-288.
[42] L.i. Li, Y. Hu, L. Ling, Wave propagation in viscoelastic single-walled carbon nanotubes with surface effect under magnetic field based on nonlocal strain gradient theory, Physica E: Low-dimensional Systems and Nanostructures, 75 (2016) 118-124.
[43] L.i. Li, Y. Hu, Buckling analysis of size-dependent nonlinear beams based on a nonlocal strain gradient theory, International Journal of Engineering Science, 97 (2015) 84-94.
[44] A. Farajpour, M.R.H. Yazdi, A. Rastgoo, M. Mohammadi, A higher-order nonlocal strain gradient plate model for buckling of orthotropic nanoplates in thermal environment, Acta Mechanica, (2016) 1-19.
[45] L.i. Li, Y. Hu, L. Ling, Flexural wave propagation in small-scaled functionally graded beams via a nonlocal strain gradient theory, Composite Structures, 133 (2015) 1079-1092.
[46] L.i. Li, X. Li, Y. Hu, Free vibration analysis of nonlocal strain gradient beams made of functionally graded material, International Journal of Engineering Science, 102 (2016) 77-92.
[47] F. Ebrahimi, M.R. Barati, A. Dabbagh, A nonlocal strain gradient theory for wave propagation analysis in temperature-dependent inhomogeneous nanoplates, International Journal of Engineering Science, 107 (2016) 169-182.
[48] S. Faroughi, S.M.H. Goushegir, H.H. Khodaparast, M.I. Friswell, Nonlocal elasticity in plates using novel trial functions, International Journal of Mechanical Sciences, 130 (2017) 221-233.
[49] L. Behera, S. Chakraverty, Effect of scaling effect parameters on the vibration characteristics of nanoplates, Journal of Vibration and Control, 22 (2016) 2389-2399.
[50] L. Behera, S. Chakraverty, Free vibration of nonhomogeneous Timoshenko nanobeams, Meccanica, 49 (2014) 51-67.
[51] S. Chakraverty, L. Behera, Free vibration of rectangular nanoplates using Rayleigh–Ritz method, Physica E: Low-dimensional Systems and Nanostructures, 56 (2014) 357-363.
[52] R.D. Mindlin, Micro-structure in linear elasticity, Archive for Rational Mechanics and Analysis, 16 (1964) 51-78.
[53] R.D. Mindlin, Second gradient of strain and surface-tension in linear elasticity, International Journal of Solids and Structures, 1 (1965) 417-438.
[54] C.M. Wang, J.N. Reddy, K.H. Lee, Shear deformable beams and plates: Relationships with classical solutions, Elsevier, 2000.

[55] M.R.K. Ravari, H. Zeighampour, Vibration analysis of functionally graded carbon nanotube-reinforced composite nanoplates using Mindlin's strain gradient theory, Composite Structures, 134 (2015) 1036-1043.
[56] M. Mohr, J. Maultzsch, E. Dobardžić, S. Reich, I. Milošević, M. Damnjanović, A. Bosak, M. Krisch, C. Thomsen, Phonon dispersion of graphite by inelastic x-ray scattering, Physical Review B, 76 (2007) 035439.
[57] L.E. Shen, H.S. Shen, C.L. Zhang, Nonlocal plate model for nonlinear vibration of single layer graphene sheets in thermal environments, Computational Materials Science, 48 (2010) 680-685.